UTRECHT UNIVERSITY

MASTER'S THESIS

MSC THEORETICAL PHYSICS

Modelling a bioelectrochemical cell from a physics perspective

Author:
Egbert Loeffen

Supervisor:
Prof. dr. René van Roij

Institute for Theoretical Physics

January 29, 2021

Bioelectrochemical cells utilize bacteria in order to extract electricity from organic compounds, for example found in wastewater streams. This process occurs within a thin layer of bacterial cells, the biofilm, on either the anode or cathode. Using a physics based modelling approach, four main processes in the (anode) biofilm are considered; ionic transport coupled to acid-base reactions, biochemical conversion of acetate species, electron transfer to a network of conductive pili, and charge transport through the pili towards the electrode. Results obtained by De Lichtervelde et al. [*Physical Review Applied*, vol. 12, no. 1, p. 014 018, 2019] are replicated, showing a reproducibility of the model. These results indicate that an accumulation of protons within the biofilm limits the current that can be extracted from the bioelectrochemical cell. Based on the electric potential profile within the biofilm, the question arises if the local electroneutrality condition can be used within these kinds of systems. To investigate this, a first attempt in adding the Poisson equation to the system is made. Based on length-scale considerations, the results obtained from using the local electroneutrality condition seem reliable, but the potential profile should be interpreted with caution.

Contents

1. Introduction

In 2015, the United Nations created 17 Sustainable Development Goals as a universal agenda for sustainable development [1]. These 'global goals' identify areas of critical importance for the world in the next 15 years. Two goals are providing clean energy and clean water for all. A promising technology that can contribute to both these goals is that of bioelectrochemical systems. These systems can use wastewater as input for producing electricity, while cleaning the water simultaneously [2].

In recent years, research on bioelectrochemical systems has increased and these systems have potential to be used in various applications, ranging from electricity production, creation of chemicals such as hydrogen and nitrogen gas, and wastewater treatment [3]–[6]. However, for these systems to be implemented on a large scale, more developments must first be made [3], [7].

In general, an electrochemical system consists of two electrodes, an anode and a cathode, seperated by a medium. At the anode, an excess of electrons is created, which is transported through an external circuit to the cathode, where the electrons can be used in various ways (e.g. to produce certain chemicals or their electric energy is used directly). Specifically, a bioelectrochemical system utilizes microorganisms either on the anode or cathode in order to catalyze certain reactions [8], [9]. This happens within a layer that is present on either (or both) electrode(s), which is called the biofilm. In section 2, more detailed information will be given on the (bio)electrochemical system and its various applications.

The focus of this thesis is analyzing the biofilm of the anode from a physics perspective. This modeling approach was taken by De Lichtervelde *et al.* [9] and will be taken as a starting point for further developments. The main goal is to investigate whether the local electroneutrality condition that is used in the original model is consistent with the results that were obtained. This will be done in several steps. Firstly, in section 2, relevant background information will be discussed. Thereafter, the model of De Lichtervelde *et al.* [9] will be discussed in section 3. In section 4, an alteration of the original model, in which the local electroneutrality condition is removed, is presented. Lastly, in section 5, the conclusions of this thesis are discussed and suggestions for improvements are made.

2. Background Information

In this section, we will discuss all relevant background information needed to model a typical bioelectrochemical system. First, we will look at the various components of the (bio)electrochemical cell and its applications. Next, we will focus on the biofilm and describe the main processes that take place. This section will contain the main theoretical considerations upon which this thesis is built.

2.1 The electrochemical cell

In general, an electrochemical cell is a system which can either extract electric energy from chemical reactions or use electric energy to drive otherwise non-spontaneous chemical reactions [10]. The first class can be further split up into two types of cells, the voltaic cell and the fuel cell, while the second class is called the electrolytic cell. We will discuss all three types in more detail.

Firstly, the voltaic cell extracts electric energy from a system through spontaneous reactions taking place. It is a closed system, consisting of two different electrodes immersed in electrolytes, which are connected through an external circuit [10]. These two electrodes are called the anode, which attracts negative ions, and the cathode, which attracts positive ions. Within the system there is a membrane or bridge which allows certain ionic species, depending on the type of reactions taking place, to flow from one electrode to the other. The entire system can be seen in figure 2.1a, in which the anode is taken to be zinc and the cathode to be copper.

The process through which the voltaic cell releases electric energy is based on chemical reactions [10]. On the anode, spontaneous chemical reactions take place, which create an excess of electrons. These electrons are transported through the external circuit to the cathode, where they are used in another chemical reaction. In the external circuit, the electric energy from the electrons can be used. If the species involved in the chemical reactions run out, then no more excess electrons can be extracted and the voltaic cell does not produce electricity anymore.

In contrast to the voltaic cell, a fuel cell can continuously produce electric energy [10], [13]. This is due to an inflow and outflow of species, ensuring that chemicals do not run out and that excess chemicals are transported away. Its set-up is shown in figure 2.1b, in which one can see two electrodes within an electrolyte connected by an external circuit, and an in- and outflow of species on either side of the electrodes. In the figure, an example of a fuel cell using hydrogen and oxygen is given.

Lastly, the electrolytic cell works in the opposite way, using electric energy to drive chemical reactions [14]. The set-up of an electrolytic cell is the same as a voltaic cell, except that the external circuit is connected to a power source such that electric energy goes into the system. The reactions happening within the electrolytic cell are non-spontaneous reactions, which only occur due to the electric energy going into the system. This system is for instance used to produce hydrogen [14].

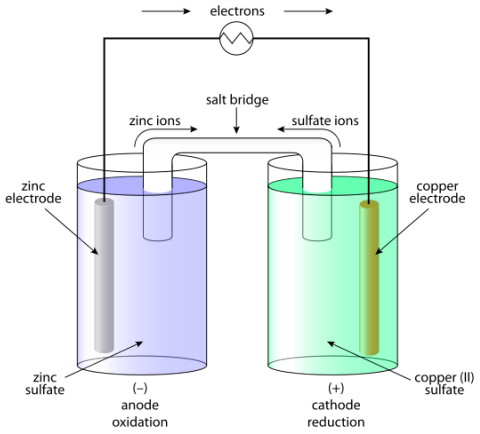

(A) An overview of the voltaic cell consisting of two electrodes, a zinc anode and a copper cathode, each submerged in electrolyte, an external circuit through which electrons flow, and a salt bridge though which ions flow. [11]

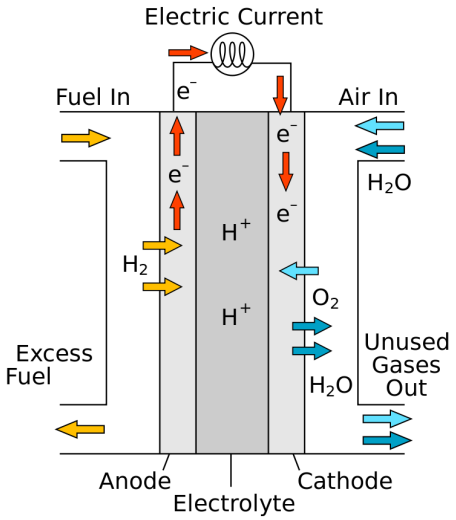

(B) An overview of the fuel cell consisting of two electrodes within an electrolyte, connected by an external circuit with a fuel inflow of hydrogen and oxygen and a fuel outflow of excess species. [12]

FIGURE 2.1: An overview of the voltaic cell (2.1a) and the fuel cell (2.1b).

2.1.1 The bioelectrochemical cell

In the electrochemical systems discussed so far, there is no biological aspect involved; the reactions occur spontaneously or are driven by an external power source. In a bioelectrochemical system, some reactions are catalyzed by microorganisms [9]. This is done in a so called biofilm, which is a layer of microorganisms on an electrode. Chemical species within the electrolyte will be transported through the biofilm, so that the microorganisms can catalyze reactions involving these species. The biofilm can be present on either the anode or the cathode (or both), resulting in a bioanode or biocathode [9].

The biofilm that is considered in this thesis consists of three main parts; the bacterial cells, the extracellular space, and the pili. The bacteria are of the *Geobacter* type, which have the property of creating a conductive network outside of the bacterial cell, the pili [15]–[17]. This can be seen in figure 2.2, where an image of the bacteria along with its network of conductive pili can be seen. The wires can transport charge towards the electrode, resulting in thicker biofilms and more electricity production as opposed to biofilms without pili, where electron transfer only takes place at the electrode. A typical thickness of the biofilm can be of the order of 100 μm [18].

A model of the biofilm used in this thesis can be seen in figure 2.3 [9]. Note that this is a focus on the anode only; the cathode and electrolyte are not depicted, but are also present in the system. Four main processes (denoted by A, B, C, and D) occurring in the biofilm are identified. Firstly, there is transport of species through the aqueous phase outside of the bacteria. Secondly, the bacteria catalyze reactions involving acetate (Ac^- or CH_3COO^-), which we define to be the substrate. Thirdly, through various biochemical reactions within the bacterial cell, an excess of electrons is created, which is transferred to the pili. Lastly, charge flows through the pili to the electrode. In the next section, we will discuss all background information required to model these four processes.

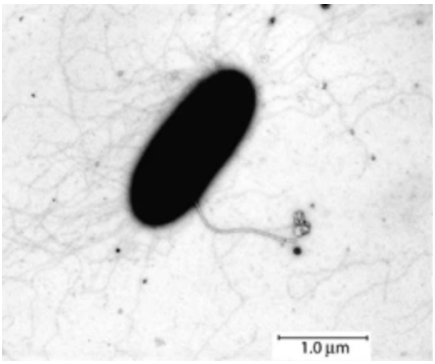

FIGURE 2.2: The *Geobacter* type bacterial cell with its network of conductive pili (the dark lines outside of the bacterial cell) [19].

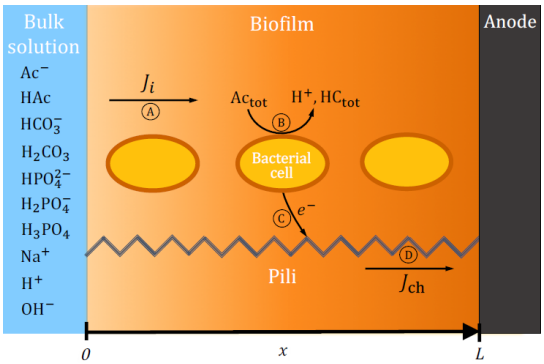

FIGURE 2.3: Overview of the anode biofilm in contact with a dilute bulk solution with four main processes; (A), ion transport through the biofilm, with J_i the flux of species i (mol m^{-2} s^{-1}); (B), bacterial reactions involving Ac^- or HAc, grouped together as Ac_{tot}; (C), electron transfer from the bacterial cell to a network of conductive pili; (D), transport of the charge to the electrode, with J_{ch} the current density (A m^{-2}) [9].

2.2 Physical processes within the biofilm

In this section we will present the physics needed to describe the biofilm. This will be done in four parts; ionic transport processes, the Poisson equation, (bio)chemical reactions, and electrochemical reactions.

2.2.1 Ionic transport processes[1]

When describing a system involving ionic species, one must understand how such species behave in solution. In any system, there are various forces acting upon particles, such as collisions with other particles or electrostatic forces. In order to describe the effect of these forces, we define the mobility μ (s kg^{-1}) as the velocity v (m s^{-1}) that a particle acquires when acted upon by a unit force F (N);

$$\mu = \frac{v}{F}. \tag{2.1}$$

As a first approximation in describing ion transport, let us first ignore electrostatic forces. Therefore, we only look at diffusion, with a force acting upon particles due to an osmotic pressure difference. Consider a cylinder with area A and width dx. Particles of species i feel a diffusion force Adp_i, due to the difference in osmotic pressure dp_i measured over the interval dx. Note that the force on the particles is in the opposite direction as the difference in osmotic pressure. The number of particles in the slice is given by $c_i N_A A dx$, with c_i the concentration of species i (mol m^{-3}) and N_A Avogradro's number (mol^{-1}). Combining this, we find that the force per particle F is given by

$$F = -\frac{Adp_i}{Ac_i N_A dx} = -\frac{1}{N_A c_i}\frac{dp_i}{dx}. \tag{2.2}$$

Using equation 2.1, we thus find that the velocity of each particle of species i is given by

$$v_i = -\mu_i \frac{1}{N_A c_i}\frac{dp_i}{dx}, \tag{2.3}$$

with μ_i the mobility of species i.

We can now translate the velocity of each particle to the total flux J_i (mol m^{-2} s^{-1}) of species i by multiplying the velocity of each particle v_i with the concentration c_i of species i, $J_i = v_i c_i$. Using the ideal gas law ($p_i = c_i k_B T N_A$), we find

$$J_i = -\mu_i k_B T \frac{dc_i}{dx}, \tag{2.4}$$

with k_B Boltzmann's constant (J K^{-1}) and T the temperature (K). Note that by using the ideal gas law, this equation holds in the dilute solution limit.

Equation 2.4 describes transport of particles behaving as an ideal gas by diffusion, which is also given by Fick's law,

$$J_i = -D_i \frac{dc_i}{dx}, \tag{2.5}$$

with D_i the diffusion coefficient (m^2 s^{-1}). By using equations 2.4 and 2.5, we can relate the mobility μ_i to the diffusion coefficient D_i as $D_i = \mu_i k_B T$, which is used more commonly and can be measured experimentally.

[1] This section is largely based on [20] and [21].

We can also include the effect of an electric field on the transport of ionic species. The electric force F_{el} acting upon a single ion in an electric field $E = -\frac{d\psi}{dx}$ (with ψ the electric potential (V)), is given by

$$F_{el} = -z_i e \frac{d\psi}{dx}, \tag{2.6}$$

with z_i the valency and e the elementary (proton) charge (C). Using equation 2.1, we find that the velocity of each particle due to the electric force $v_{i,el}$ is given by $v_{i,el} = -\mu_i z_i e \frac{d\psi}{dx}$. The flux $J_{i,el}$ due to this electric force is given by

$$J_{i,el} = v_{i,el} c_i = -\mu_i z_i e c_i \frac{d\psi}{dx}. \tag{2.7}$$

Combining equation 2.4 and 2.7, we find the total flux of ionic species i due to osmotic pressure and an electric field to be

$$\begin{aligned} J_i &= -\mu_i \left(k_B T \frac{dc_i}{dx} + z_i e c_i \frac{d\psi}{dx} \right) \\ &= -D_i \left(\frac{dc_i}{dx} + z_i c_i \frac{e}{k_B T} \frac{d\psi}{dx} \right), \end{aligned} \tag{2.8}$$

where in the second line we have substituted the expression for the diffusion coefficient. Note that the derivation of this equation is done in one dimension, but can be generalized to hold in all three spatial dimensions.

Equation 2.8 is known as the Nernst-Planck equation and is used to describe transport of ionic species in dilute solutions. It consists of a diffusion term and a conduction term. A convection term can also be added when considering an overall fluid flow. The Nernst-Planck equation will be used throughout this thesis.

2.2.2 The Poisson Equation[2]

A system in which electric charges are present is affected by the electric potential. For example, if an electric field is imposed in a conductor of free charge carriers, all positive charges will tend to move with the electric field, while negative charges will tend to move opposite to the electric field. An electric field $\mathbf{E}$ is the negative spatial derivative of the electric potential ψ,

$$\mathbf{E} = -\nabla \psi. \tag{2.9}$$

Therefore, it is important to accurately describe the potential within a system. The relation between the (local) electric charge in a system and the electric potential is given by the Poisson equation,

$$\nabla^2 \psi = -\frac{\rho}{\epsilon}, \tag{2.10}$$

with ρ (C m^{-3}) the charge density and ϵ (F m^{-1}) the permittivity, which is a material dependent property.

One important consequence of the Poisson equation in an electrolyte is the formation of electric double layers. These are layers of ions near a charged surface that screen the potential at this surface. Consider a system consisting of two monovalent pointlike species of ions of charge $\pm e$ in contact with a charged surface at $z = 0$ with surface charge density $e\sigma$ (C m^{-2}). Far away from the surface, the particles have a

[2]This section is largely based on [20]

total bulk salt concentration of $2\rho_s$ (m^{-3}). The Poisson equation in this geometry is given by

$$\frac{d^2\psi}{dz^2} = -\frac{e}{\epsilon}(\rho_+(z) - \rho_-(z)), \tag{2.11}$$

with ρ_+, ρ_- (m^{-3}) the number density of the cations and anions, respectively. Using mean-field Boltzmann distributions, the cation and anion density is given by

$$\rho_\pm(z) = \rho_s e^{\mp\frac{e\psi(z)}{k_B T}} = \rho_s e^{\mp\phi(z)}, \tag{2.12}$$

with ρ_s the bulk salt concentration (m^{-3}) and where we have defined the dimensionless electric potential $\phi = \frac{e\psi}{k_B T}$. In this Boltzmann distribution, the energy of an ion with charge $\pm e$ is approximated by its electric energy $\pm e\psi$.

In order to solve equation 2.11, we need two boundary conditions. The first boundary condition is given by the potential far away from the surface, which must approach zero,

$$\lim_{z\to\infty} \psi(z) = 0. \tag{2.13}$$

The second boundary condition is given by total charge neutrality; the total charge density in the system must be opposite to the total charge density imposed on the surface. This condition is given by

$$\begin{aligned}\sigma &= -\int_0^\infty dz(\rho_+(z) - \rho_-(z)) \\ &= \frac{\epsilon}{e}\int_0^\infty dz \frac{d^2\psi(z)}{dz^2} \\ &= -\frac{\epsilon}{e}\frac{d\psi(0)}{dz},\end{aligned} \tag{2.14}$$

where we have used equation 2.11 in the second line, and 2.13 in the last line. Recognizing the sin hyperbolic, we can rewrite this system as

$$\begin{aligned}\frac{d^2\phi(z)}{dz^2} &= \lambda_D^{-2}\sinh(\phi(z)) \\ \phi(z\to\infty) &= 0 \\ \frac{d\phi}{dz}(0) &= -4\pi\lambda_B\sigma,\end{aligned} \tag{2.15}$$

where we have defined two length scales, the Debye length λ_D (m) and the Bjerrum length λ_B (m), given by

$$\begin{aligned}\lambda_D &= \left(\frac{\epsilon k_B T}{2e^2\rho_s}\right)^{1/2} \\ \lambda_B &= \frac{e^2}{4\pi\epsilon k_B T}.\end{aligned} \tag{2.16}$$

These two length scales are characteristic length scales of the system. The Bjerrum length is a property of the solvent and it gives the distance over which the Coulomb interaction between two unit charges is equal to $k_B T$. The Debye length is a function of the salt concentration and gives the length scale on which charge imbalance persists. At distances from the surface much larger than the Debye length, there is an approximate charge balance within the system.

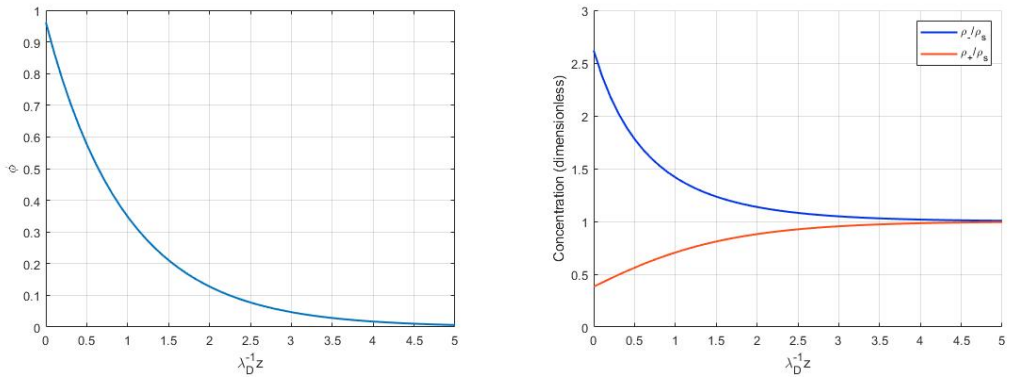

FIGURE 2.4: The dimensionless potential profile $\phi(z)$ (left) and the dimensionless concentration profiles of the cation $\rho_+(z)/\rho_s$ and anion $\rho_-(z)/\rho_s$ (right) as function of distance in units of Debye length for $y = 1$.

The Debye length can be visualized by looking at the electrostatic potential and density profiles. The potential can be obtained by solving the Poisson-Boltzmann equation, equation 2.15, giving

$$\phi(z) = 2 \ln \frac{1 + \gamma e^{-z/\lambda_D}}{1 - \gamma e^{-z/\lambda_D}}, \tag{2.17}$$

with γ an integration constant determined from

$$\frac{d\phi}{dz}(0) = \frac{-4\gamma\lambda_D^{-1}}{1 - \gamma^2} = -4\pi\lambda_B\sigma. \tag{2.18}$$

Defining the dimensionless surface charge $y = 4\pi\lambda_B\lambda_D\sigma$, we find

$$\gamma = \frac{\sqrt{1 + (y/2)^2} - 1}{y/2}. \tag{2.19}$$

We can see that λ_D gives the characteristic length scale for decay of the potential from its surface value by looking at the far-field solution ($z/\lambda_D \gg 1$), given by

$$\phi(z) \approx 4\gamma e^{-z/\lambda_D}, \tag{2.20}$$

where we can clearly see the exponential decay with length scale λ_D.

The potential profile $\phi(z)$ can be used to describe the concentration profiles,

$$\rho_\pm(z) = \rho_s \left(\frac{1 \mp \gamma e^{-z/\lambda_D}}{1 \pm \gamma e^{-z/\lambda_D}} \right)^2, \tag{2.21}$$

where again the characteristic length scale λ_D can be observed.

In figure 2.4, the potential and concentration profiles can be seen for $y = 1$. It can clearly be observed that the Debye length gives a measure of the distance at which charge imbalance is present within the system. This so called electric double layer thus acts as a screening layer for the charge density that is present on the surface. Any charged surface in contact with an electrolyte will be screened through this mechanism. This will be used to describe the biofilm model in section 4.

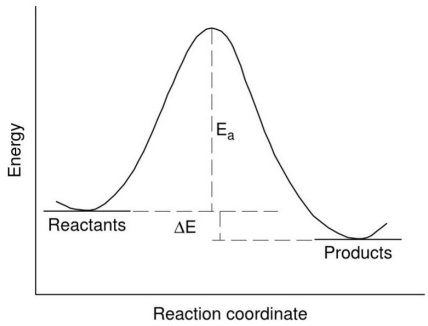

FIGURE 2.5: Energy of the steps in a reaction chain where reactants are separated from the products, with an energy difference ΔE, by an energy barrier with an activation energy E_a. The reaction coordinate indicates the state of the reaction. [22]

2.2.3 Reaction kinetics[3]

When working on a system involving reactions, the rate at which a reaction takes place is of importance. For a general reaction $a\mathrm{A} + b\mathrm{B} \rightarrow c\mathrm{C} + d\mathrm{D}$, the reaction rate r (mol m^{-3} s^{-1}), defined as $r \equiv -\frac{1}{a}\frac{d[\mathrm{A}]}{dt}$, with $[\mathrm{A}]$ the concentration of species A (mol m^{-3}) and t the time (s), can be described by

$$r = k[\mathrm{A}]^a[\mathrm{B}]^b, \tag{2.22}$$

where k is the rate constant (dimension depends on specific reaction). More (or less) factors can be included if more (or less) reactants are involved in the reaction. The value of a and b indicate the order of the reaction.

For a first-order reaction, take for example $\mathrm{A} \rightarrow \mathrm{B}$, we can integrate the rate equation $r = -\frac{d[\mathrm{A}]}{dt} = k[\mathrm{A}]$ to obtain

$$[\mathrm{A}] = [\mathrm{A}]_0 \mathrm{e}^{-kt}, \tag{2.23}$$

which describes how the concentration of species A decreases over time starting from an initial concentration $[\mathrm{A}]_0$. The rate constant k can for instance be determined experimentally, but its temperature dependence is often described by the Arrhenius equation,

$$k = C\mathrm{e}^{-E_a/k_B T}. \tag{2.24}$$

In this equation, C is an exponential prefactor with the same dimension as the rate constant, E_a is the activation energy (J), k_B the Boltzmann constant (J K^{-1}) and T the temperature (K). The key part of this equation is that there is some energy barrier which needs to be overcome for the reaction to take place. This can be seen in figure 2.5, where an energy barrier E_a separates the reaction products from the reactants. Even though the final energy of the products is lower than the energy of the reactants, represented by ΔE, the activation energy must be overcome. The prefactor C can be interpreted as the frequency of collisions in the correct orientation, with the exponential describing the probability of the reaction occurring given such a perfect collision.

In equilibrium, where both a forward and a backward reaction takes place, instead of using the two separate rate constant for each reaction, one often simply

[3] This section is largely based on [22].

takes one equilibrium constant. This is because often the two rate constants themselves cannot be determined experimentally, only their ratio. Suppose we have the system

$$aA + bB \underset{k_{-1}}{\overset{k_1}{\rightleftharpoons}} cC \tag{2.25}$$

with k_1 the rate constant for the forward reaction and k_{-1} for the backward reaction. Assuming that the coefficients a, b, and c represent the order of the reaction, the production rate r_i for each species i is given by

$$\begin{aligned} r_A &= r_B = k_{-1}[C]^c \\ r_C &= k_1[A]^a[B]^b. \end{aligned} \tag{2.26}$$

Since both the forward and backward reaction occur simultaneously, the rate constants cannot simply be determined experimentally. However, in equilibrium, we know that there is no net production of any species, so by setting $r_A = r_C$, we find

$$K \equiv \frac{k_{-1}}{k_1} = \frac{[A]^a[B]^b}{[C]^c}, \tag{2.27}$$

where K is defined as the equilibrium constant, with dimension mol m^{-3} for $a = b = c = 1$. As equation 2.27 must hold in equilibrium, we can determine the value of the equilibrium constant by measuring the equilibrium concentrations. However, since equation 2.27 contains three unknown concentrations, it cannot be used to solve for equilibrium concentrations. Therefore, often more information about the system is needed, such as the total concentration of two species (e.g. $[A] + [C] = constant$).

In literature, sometimes instead of the value of K, the value of pK is given, with $k = 10^{-pK}$. By comparing the order of the concentrations of the species with the pK value, one can estimate which reaction is dominant in an out-of-equilibrium situation. For example, if the order of concentration of the products is much higher than the pK, the backward reaction will be dominant.

Biochemical systems

In biochemical systems, an enzyme is often included in a reaction sequence. Often, the substrate (S) binds with the enzyme (E) forming an enzyme-substrate complex (ES), after which the enzyme is released together with a product (P). This is described by

$$E + S \underset{k_{-1}}{\overset{k_1}{\rightleftharpoons}} ES \underset{k_{-2}}{\overset{k_2}{\rightleftharpoons}} E + P \tag{2.28}$$

with k_1 and k_2 the rate constants for the forward reactions and k_{-1} and k_{-2} the rate constants for the backward reactions. It is of interest to find the rate at which the product is formed, which is now not simply dependent on one rate constant. In most cases, the concentration of the product is low and the backward reactions from the product can be neglected. Therefore, we set $k_{-2} = 0$, making the system irreversible. In steady state, there will be no net creation of the enzyme-substrate complex, so we can say that the production of ES must be equal to the decomposition of ES,

$$k_1[E][S] = k_{-1}[ES] + k_2[ES], \tag{2.29}$$

where [..] indicates the concentration of the species within the brackets (mol m^{-3}).

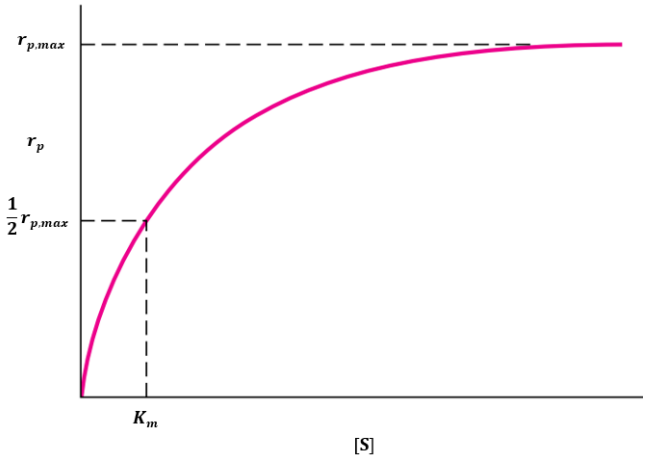

FIGURE 2.6: Reaction rate r_p as function of substrate concentration [S], where the Michaelis-Menten constant K_m indicates at which substrate concentration the reaction rate is half of its maximum value (adapted from [23]).

We do not know the concentration of either the enzyme or the enzyme-substrate complex, but often we do know the total concentration of the enzyme $[E]_t \equiv [E] + [ES]$, which does not change throughout the reaction. Substituting $[E] = [E]_t - [ES]$ in equation 2.29, we can find that the enzyme-substrate complex concentration in equilibrium must be

$$[ES] = \frac{k_1[E]_t[S]}{k_{-1} + k_2 + k_1[S]}. \tag{2.30}$$

We can use this concentration to find the production rate of the product r_p as in reaction 2.28, which is given by

$$r_p = k_2[ES] = \frac{k_1 k_2[E]_t[S]}{k_{-1} + k_2 + k_1[S]}. \tag{2.31}$$

Defining the Michaelis-Menten constant $K_m \equiv \frac{k_{-1}+k_2}{k_1}$, we arrive at

$$r_p = \frac{k_2[E]_t[S]}{K_m + [S]} \approx \begin{cases} \frac{k_2[E]_t}{K_m}[S] & \text{for } [S] \ll K_m \\ \frac{k_2[E]_t}{K_m} & \text{for } [S] \gg K_m \end{cases} \tag{2.32}$$

We can understand what the Michaelis-Menten constant describes by looking at the behaviour of r_p for various substrate concentrations, which is plotted in figure 2.6. It can be seen that for low substrate concentrations ($[S] \ll K_m$), we have a linear dependence of the reaction rate on the substrate concentration ($r_p \propto [S]$), indicating a first order reaction. At high substrate concentrations ($[S] \gg K_m$), we have no dependence of the reaction rate on the substrate concentration ($r_p \propto \frac{k_2[E]_t}{K_m}$, indicating a zeroth order reaction. At the point where the substrate concentration is equal to the Michaelis-Menten constant, the reaction rate is half of its maximum value, $r_p = \frac{1}{2}\frac{k_2[E]_t}{K_m}$. Therefore, the Michaelis-Menten constant gives the concentration of the substrate for which the production rate of P is half of its maximum value.

2.2.4 Electrochemical reactions[4]

All reactions that involve the transfer of charge (electrons) to or from an electrode are called electrochemical reactions. The energy needed to add one electron to a metal, also called the Fermi level, is dependent on the potential, so by controlling the electrode potential, the electron energy within the electrode can be altered. By doing so, the direction of the electrochemical reaction can be altered. If the electron energy is lowered (i.e. a higher electrode potential), electrons are 'more eager' to move to the electrode and the reaction is driven in the direction where free electrons are created. To look at this process in more detail, let us consider a general reaction where n electrons are created:

$$\mathrm{Re} \underset{k_{-1}}{\overset{k_1}{\rightleftharpoons}} \mathrm{Ox} + n\mathrm{e}^- \tag{2.33}$$

with Re being the reduced states, Ox the oxidized states, n the number of electrons transferred to the electrode, e^- the electron, k_1 the forward reaction rate, and k_{-1} the backward reaction rate.

We are interested in determining at what rate electrons are transferred to the electrode, which is given by the current density i (A m^{-2}). Note that the current density is more interesting than the current itself, since the electrochemical reaction (reaction 2.33) occurs everywhere on the surface of the electrode, which means that a doubling of the electrode surface area results in a doubling of the current. In each reaction, n electrons are created, so the current density i is given by

$$i = -ner, \tag{2.34}$$

with r the reaction rate per unit area (s^{-1} m^{-2}) and e the elementary charge (C). Note that the minus sign is needed for a correct sign of the current; if the reaction rate is positive, electrons are transferred to the electrode, so the current flows into the electrolyte (negative). This reaction rate is the *net* reaction rate, which is given by the difference between the forward and the backward reaction rate. Using equation 2.22, we find

$$\begin{aligned} r &= k_1[\mathrm{Re}] - k_{-1}[\mathrm{Ox}] \\ &= C_1[\mathrm{Re}]\mathrm{e}^{-E_{a,Re}/k_BT} - C_{-1}[\mathrm{Ox}]\mathrm{e}^{-E_{a,Ox}/k_BT} \end{aligned} \tag{2.35}$$

with [Re] and [Ox] the surface concentration of the reduced and oxidized states respectively and where in the second line we have used the Arrhenius equation (eqation 2.24) to show the exponential dependence of the rate constants (C_1 and C_{-1} are the exponential prefactors, and $E_{a,Re}$ and $E_{a,Ox}$ the activation energy (J) of the forward and backward reaction, respectively).

The activation energy of the forward and backward reaction is initially not the same, as can be understood from figure 2.5. For the forward reaction, the activation energy is given by $E_{a,Re} = E_a$, while the activation energy for the backward reaction is given by $E_{a,Ox} = E_a + \Delta E$. However, in an electrochemical reaction, there will be a built-up of charge, due to the electrons being in the electrode while the oxidized state remains in the electrolyte. This will result in a potential gradient over the electrode interface. This potential gradient will slow down the forward reaction until the forward and backward reaction are in balance; we obtained steady-state.

[4]This section is largely based on [13], [24], and [25].

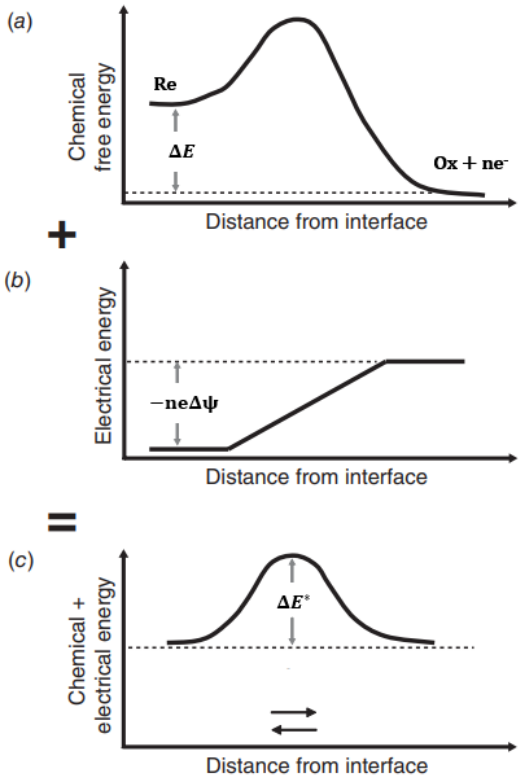

FIGURE 2.7: In equilibrium, the chemical energy difference between the oxidized and reduced state (part a) is counteracted by the electric energy difference (part b) resulting in an equal energy barrier ΔE^* (part c) and thus a net zero reaction rate (adapted from [13]).

In figure 2.7, the difference in chemical energy and electric energy is presented. In part a, it can be seen that the oxidized state represents a lower chemical energy, resulting in a lower activation energy for the forward reaction (the barrier as approached from the left) than for the backward reaction (the barrier as approached from the right). However, as can be seen in part b, this results in a potential gradient, due to an accumulation of electrons in the electrode, which balances the activation energy difference, resulting in a net equal activation energy ΔE^* as can be seen in part c. Note that on the horizontal axis, the distance from the interface is presented, which is of the order of nanometers. The potential drop happens right at the electrode-electrolyte interface.

Since the potential alters the activation energy, the current density can be affected by altering the electrode potential. By doing so, one can obtain a net current through the electrode. This can be described by looking at the energy of three distinct states, the reduced state (E_{Re}), the oxidized state (E_{Ox}), and the transition state (E_T). All three states have a chemical energy (J), indicated by U_{Re}, U_{Ox}, and U_T respectively, which is independent of the potential. In addition, all three states have an electric energy (J), given by the charge multiplied by the electric potential ψ. The charge of the reduced state is denoted by q_{Re} (C) and the charge of the oxidized state (excluding the n electrons in the electrode) is denoted by q_{Ox}. Note that by charge conservation we have $q_{Re} = q_{Ox} - ne$, with e the elementary charge (C).

We can now describe the total energy of the reduced and oxidized state, which is given by

$$\begin{aligned} E_{Re} &= U_{Re} + q_{Re}\psi \\ E_{Ox} &= U_{Ox} + q_{Ox}\psi - ne\psi_e, \end{aligned} \tag{2.36}$$

with ψ_e the electric potential in the electrode (V). Note that the electric energy from the electrons is determined with the electrode potential, since the electrons are located in the electrode. Also note that the potential ψ is the potential a few nanometer in the electrolyte, see figure 2.7.

Using the Butler-Volmer assumption, the electric energy of the transition state is given by an α-weighted average over the electric energy of the oxidized and reduced states. This α is called the transfer coefficient or symmetry factor, with a value between 0 and 1 (typically around 0.5). It describes how much of the electric energy of the transition state comes from the reduced state. Using this, the total energy of the transition state is given by

$$E_T = U_T + \alpha q_{Re}\psi + (1-\alpha)(q_{Ox}\psi - ne\psi_e). \tag{2.37}$$

We can now substitute the activation energies in equation 2.35 using $E_{a,Re} = E_T - E_{Re} = U_T - U_{Re} - ne(1-\alpha)(\psi_e - \psi)$ and $E_{a,Ox} = E_T - E_{Ox} = U_T - U_{Ox} + \alpha ne(\psi_e - \psi)$, which gives

$$r = C_1[\mathrm{Re}]e^{(-U_T+U_{Re}+ne(1-\alpha)(\psi_e-\psi))/k_BT} - C_{-1}[\mathrm{Ox}]e^{(-U_T+U_{Ox}-\alpha ne(\psi_e-\psi))/k_BT}. \tag{2.38}$$

Since there is no dependence on the electric potential in the chemical energies, we can absorb the exponential factor into the definition of the exponential prefactors C_1 and C_{-1}. Defining $C_1^* \equiv C_1 e^{(-U_T+U_{Re})/k_BT}$, $C_{-1}^* \equiv C_{-1}e^{(-U_T+U_{Ox})/k_BT}$, and defining the difference in electrode potential and the potential in the electrolyte as $\Delta\psi \equiv$

$\psi_e - \psi$, we obtain

$$r = C_1^*[\mathrm{Re}]e^{ne(1-\alpha)\Delta\psi/k_BT} - C_{-1}^*[\mathrm{Ox}]e^{-\alpha ne\Delta\psi/k_BT}. \tag{2.39}$$

In equilibrium, a potential difference $\Delta\psi_{eq}$ will ensure that the net reaction rate per unit area is zero. Solving $r = 0$ in equation 2.39 for $\Delta\psi_{eq}$, we obtain

$$\Delta\psi_{eq} = \frac{k_BT}{ne}\ln\left[\frac{C_{-1}^*[\mathrm{Ox}]}{C_1^*[\mathrm{Re}]}\right]. \tag{2.40}$$

When one controls the electrode potential, one actually controls the difference in potential as compared to the equilibrium potential, Therefore, more commonly the overpotential $\eta \equiv \Delta\psi - \Delta\psi_{eq}$ is used instead of the potential itself. We can now describe the current density i as a function of the overpotential η. Starting from equation 2.34 and substituting equations 2.39, 2.40, and $\Delta\psi = \eta + \Delta\psi_{eq}$, we obtain

$$\begin{aligned} i &= ne(C_{-1}^*[\mathrm{Ox}]e^{-\alpha ne(\eta+\Delta\psi_{eq})/k_BT} - C_1^*[\mathrm{Re}]e^{ne(1-\alpha)(\eta+\Delta\psi_{eq})/k_BT}) \\ &= ne(C_{-1}^*[\mathrm{Ox}]\left(\frac{C_{-1}^*[\mathrm{Ox}]}{C_1^*[\mathrm{Re}]}\right)^{-\alpha}e^{-\alpha ne\eta/k_BT} - C_1^*[\mathrm{Re}]\left(\frac{C_{-1}^*[\mathrm{Ox}]}{C_1^*[\mathrm{Re}]}\right)^{1-\alpha}e^{(1-\alpha)ne\eta/k_BT} \\ &= ne(C_{-1}^*[\mathrm{Ox}])^{1-\alpha}(C_1^*[\mathrm{Re}])^{\alpha}\left[e^{-\alpha ne\eta/k_BT} - e^{(1-\alpha)ne\eta/k_BT}\right]. \end{aligned} \tag{2.41}$$

We can absorb all prefactors into the definition of the exchange current density $i_0 = ne(C_{-1}^*[\mathrm{Ox}])^{1-\alpha}(C_1^*[\mathrm{Re}])^{\alpha}$, which can by measured experimentally for a specific reaction. Using this definition we obtain the Butler-Volmer equation, which describes the current density of a certain reaction as a function of overpotential;

$$i = i_0\left[e^{-\alpha ne\eta/k_BT} - e^{(1-\alpha)ne\eta/k_BT}\right] \tag{2.42}$$

One can obtain the total current $I = iA$ (A) by multiplying the current density i with the area of the electrode A.

To understand the behaviour of the Butler-Volmer equation, we can look at the two limits; $|\eta| \ll k_BT/e$ (the low overpotential region) and $|\eta| \gg k_BT/e$ (the high overpotential region). For the low overpotential region, we can use a Taylor expansion of the exponential to obtain

$$i = -i_0\frac{ne\eta}{k_BT}. \tag{2.43}$$

We recognize a linear response for low overpotential, following Ohm's law.

For the high overpotential region, one exponential becomes negligible, depending on a negative or positive overpotential, giving

$$i = \begin{cases} -i_0e^{(1-\alpha)ne\eta/k_BT}, & \eta \gg k_BT/e \\ i_0e^{-\alpha ne\eta/k_BT}, & \eta \ll -k_BT/e. \end{cases} \tag{2.44}$$

These equations are known as the Tafel equations [26] and are more commonly written as

$$\eta = a + b\log i, \tag{2.45}$$

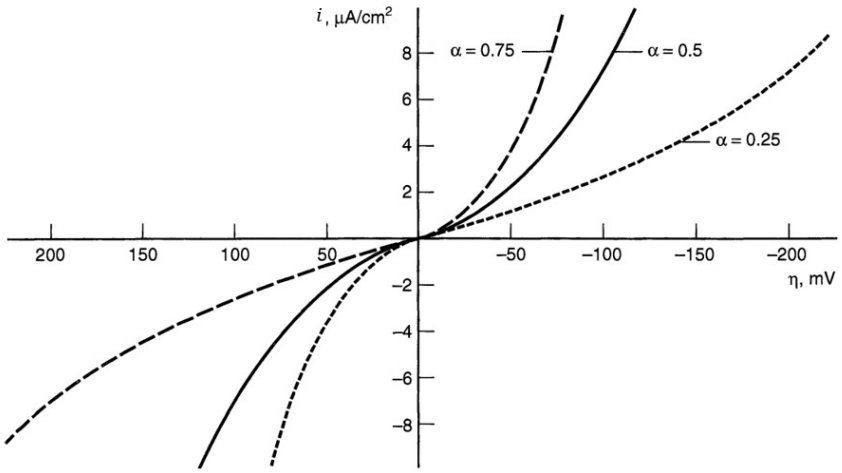

FIGURE 2.8: The current density i as a function of the overpotential η for various values of α with $n = 1$, $T = 298$ K, and $i_0 = 10^{-6}$ A/cm^2 [26].

with a and b the Tafel equation constants, whose values depend on whether a cathodic or anodic reaction is considered. For a large negative overpotential, the constants are given by

$$a = \frac{\ln(10)k_BT}{en\alpha}\log i_0 \qquad b = -\frac{\ln(10)k_BT}{en\alpha}. \tag{2.46}$$

In figure 2.8, the current density is given for various values of α as a function of the overpotential η. Both the linear response around the origin and the exponential behaviour for large η can be observed. The Butler-Volmer model will be further used throughout this thesis.

3. The Biofilm Model

In this section, the biofilm model of De Lichtervelde *et al.* [9] will be presented and discussed. By recreating the model, its results can be checked and new adaptations can be made. These adaptations will be discussed in section 4.

3.1 Model set-up

An overview of the (anode) biofilm was presented in figure 2.3 and is shown again here in figure 3.1. We assume a planar geometry and can therefore use a one-dimensional model to describe the system in terms of a single spatial variable x. The biofilm of thickness L consists of two phases; the bacterial cells and an aqueous phase outside of these cells. The ratio of the volume of the aqueous phase to the total volume of the biofilm is defined as the porosity ϵ (m^3 aqueous phase (AP)/m^3 biofilm (BF)), while the ratio of the average transport distance inside the aqueous phase to the total displacement in the biofilm is defined as the tortuosity τ (m aqueous phase (AP)/m biofilm (BF)). These characteristics are biofilm dependent.

The ionic species that are taken into account in this model represent a typical wastewater stream [9] and can be categorized in roughly two groups; organic matter, consisting of Ac^{-1}, HAc, HCO_3^-, H_2CO_3, HPO_4^{2-}, $H_2PO_4^-$, and H_3PO_4, and inorganic matter, consisting of H^+, OH^-, and Na^+. Note that more ionic species are present in the actual bulk solution, but these are grouped together within Na^+ as they are non-reactive and only the positive charge is important within the model. The driving ionic species are acetate (Ac^- or CH_3COO^- in its chemical formula) and acetic acid (HAc or CH_3COOH in its chemical formula). These species are at the beginning of the chain of reactions that will create an excess of electrons.

The main processes happening inside the biofilm will now be discussed in detail.

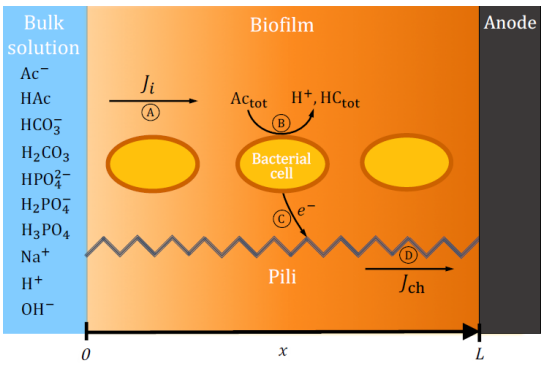

FIGURE 3.1: Overview of the anode biofilm in contact with a dilute bulk solution with four main processes; (A), ion transport through the biofilm, with J_i the flux of species i (mol m^{-2} s^{-1}); (B), bacterial reactions involving Ac^- or HAc, grouped together as Ac_{tot}; (C), electron transfer from the bacterial cell to a network of conductive pili; (D), transport of the charge to the electrode, with J_{ch} the current density (A m^{-2}) [9].

3.1.1 Ion transport through the biofilm

In the aqueous phase of the biofilm, the flux J_i of ionic species i can be described by the Nernst-Planck equation,

$$J_i = -D_{i,e}\left(\frac{\partial c_i}{\partial x} + z_i c_i \frac{\partial \phi}{\partial x}\right), \tag{3.1}$$

with $D_{i,e}$ ($m^2\ s^{-1}$) the effective diffusion coefficient and where we have defined the dimensionless potential $\phi = \frac{\psi}{V_T} = \frac{e}{k_B T}\psi$, with $V_T = \frac{k_B T}{e}$ the thermal voltage (V). The effective diffusion coefficient describes how the transport of ionic species is affected by the bacterial cells. It is given by $D_{i,e} = D_r D_i$, with $D_r = \epsilon/\tau$ the relative diffusion coefficient and D_i ($m^2\ s^{-1}$) the diffusion coefficient in free solution.

Within the biofilm, there are two type of reactions taking place; biochemical reactions due to the bacterial cells, and acid-base reactions. Taking these two sources into account, we can set up a mass balance equation for each ionic species

$$\epsilon\frac{\partial c_i}{\partial t} = -\frac{\partial J_i}{\partial x} + r_i + \gamma_i, \tag{3.2}$$

with r_i (mol $m^{-3}\ s^{-1}$) the formation rate of species i due to biochemical reactions (see section 3.1.2), and γ_i (mol $m^{-3}\ s^{-1}$) the formation rate of species i due to acid-base reactions. Note that the concentration c_i is given in mol per unit biofilm volume, while the ionic species are only present in the aqueous phase. Therefore, we need to include the factor ϵ to obtain the dimension mol per unit aqueous phase volume.

It is important to understand the difference between the biochemical reactions and the acid-base reactions. The biochemical reactions occur only when the bacterial cells are present, while the acid-base reactions occur spontaneously and at a much faster rate [27]. The following acid-base reactions are included in this model:

$$\begin{aligned} HAc &\rightleftharpoons Ac^- + H^+ \\ H_2CO_3 &\rightleftharpoons HCO_3^- + H^+ \\ H_3PO_4 &\rightleftharpoons H_2PO_4^- + H^+ \\ H_2PO_4^- &\rightleftharpoons HPO_4^{2-} + H^+ \\ H_2O &\rightleftharpoons H^+ + OH^-. \end{aligned} \tag{3.3}$$

Note that the acid-base reaction of bicarbonate to carbonate ($HCO_3^- \rightleftharpoons CO_3^{2-} + H^+$) and the acid-base reaction of hydrogen phosphate to phosphate ($HPO_4^{2-} \rightleftharpoons PO_4^{3-} + H^+$) are not included. This is because the pK values of the equilibrium constants (10.34 and 12.34 respectively [28]) are much higher than the pH considered in this system (maximum of pH 7), resulting in an equilibrium that is on the far left side of the reactions. The ionic species on the right hand side of the acid-base reactions only have significant concentrations when the pH of the solution is around or below the pK value of the specific acid-base reaction. Therefore, no significant concentration of carbonate and phosphate will be present in the system and these ionic species do not need to be considered.

We can group the ionic species together in such a way that the acid-base reactions only occur within a group. Therefore, we consider the group consisting of acetate (Ac^-) and acetic acid (HAc); the group consisting of bicarbonate (HCO_3^-) and carbonic acid (H_2CO_3); the group consisting of phosphate species (HPO_4^{2-}, $H_2PO_4^-$, and H_3PO_4); the group consisting of protons (H^+) and hydroxyl ions (OH^-); and lastly any additional unreactive ions which is described by using Na^+. Note that for the

first three groups, all γ_i sum to zero. This is because for any ion that is formed, another ion within the group is consumed. For the group consisting of protons and hydroxyl ions, this is not the case, since protons are involved in every acid-base reaction. Lastly, note that Na^+ is not present in any acid-base reaction.

For each acid-base reaction, an equilibrium condition can be created (as in equation 2.27). If we assume that the acid-base reactions are much faster than the biochemical reactions or ionic transport, which is a valid assumption [27], we can assume that the equilibrium conditions always hold. Therefore, if we know one ionic species in a group, we can directly calculate each ionic species in that group using the equilibrium conditions and the pH. Thus, we only need to consider one 'master species' per group in our model. The equilibrium conditions are given by

$$\begin{aligned} K_{\mathrm{HAc}} &= \frac{\left[\mathrm{Ac}^-\right][\mathrm{H}^+]}{[\mathrm{HAc}]} \\ K_{\mathrm{H_2CO_3}} &= \frac{\left[\mathrm{HCO_3^-}\right][\mathrm{H}^+]}{[\mathrm{H_2CO_3}]} \\ K_{\mathrm{H_3PO_4}} &= \frac{\left[\mathrm{H_2PO_4^-}\right][\mathrm{H}^+]}{[\mathrm{H_3PO_4}]} \\ K_{\mathrm{H_2PO_4}} &= \frac{\left[\mathrm{HPO_4^{2-}}\right][\mathrm{H}^+]}{\left[\mathrm{H_2PO_4^-}\right]} \\ K_{\mathrm{W}} &= \left[\mathrm{OH}^-\right]\left[\mathrm{H}^+\right], \end{aligned} \tag{3.4}$$

with K_i the equilibrium constant of the reaction involving species i and with K_W the equilibrium constant for the water self ionization reaction (the acid-base reaction involving H_2O).

Since Na^+ is not present in any reaction, its mass balance equation is given by

$$\epsilon \frac{\partial [\mathrm{Na}^+]}{\partial t} = -\frac{\partial J_{\mathrm{Na}^+}}{\partial x}, \tag{3.5}$$

with $[Na^+]$ (mol m^{-3}) the concentration of Na^+ (c_{Na^+} in equation 3.2). From now on, $[i]$ indicates the concentration of species i.

For the first three groups, we define $[\mathrm{Ac}]_{\mathrm{tot}}$, $[\mathrm{HC}]_{\mathrm{tot}}$, and $[\mathrm{H_2P}]_{\mathrm{tot}}$ to be the total concentration of species within the acetate group, the bicarbonate group, and the phosphate group respectively, given by

$$\begin{aligned} [\mathrm{Ac}]_{\mathrm{tot}} &= [\mathrm{HAc}] + \left[\mathrm{Ac}^-\right] \\ [\mathrm{HC}]_{\mathrm{tot}} &= [\mathrm{H_2CO_3}] + \left[\mathrm{HCO_3^-}\right] \\ [\mathrm{H_2P}]_{\mathrm{tot}} &= [\mathrm{H_3PO_4}] + \left[\mathrm{H_2PO_4^-}\right] + \left[\mathrm{HPO_4^{2-}}\right]. \end{aligned} \tag{3.6}$$

We can now set up a total mass balance equation by summing the individual mass balance equations per ionic species. Since the γ_i terms cancel, we are left with

$$\begin{aligned} \epsilon \frac{\partial}{\partial t} [\mathrm{Ac}]_{\mathrm{tot}} &= -\frac{\partial}{\partial x} \left(J_{\mathrm{Ac}^-} + J_{\mathrm{HAc}}\right) + r_{\mathrm{Ac_{tot}}} \\ \epsilon \frac{\partial}{\partial t} [\mathrm{HC}]_{\mathrm{tot}} &= -\frac{\partial}{\partial x} \left(J_{\mathrm{HCO_3^-}} + J_{\mathrm{H_2CO_3}}\right) + r_{\mathrm{HC_{tot}}} \\ \epsilon \frac{\partial}{\partial t} [\mathrm{H_2P}]_{\mathrm{tot}} &= -\frac{\partial}{\partial x} \left(J_{\mathrm{H_3PO_4}} + J_{\mathrm{H_2PO_4^-}} + J_{\mathrm{HPO_4^{2-}}}\right) + r_{\mathrm{H_2P_{tot}}}, \end{aligned} \tag{3.7}$$

with $r_{\mathrm{Ac_{tot}}}$, $r_{\mathrm{HC_{tot}}}$, and $r_{\mathrm{H_2P_{tot}}}$ (mol m^{-3} s^{-1}) the total production rate of acetate species, bicarbonate species, and phosphate species respectively, to be discussed in detail in section 3.1.2.

For the group involving protons and hydroxyl ions, summing the individual mass balance equations does not get rid of the γ_i. Therefore, we need another equation to fully describe the system. We consider charge conservation. At each position, the divergence of the ionic current must be equal to the rate of charge going from solution to the pili, $-r_{ch}$ (mol m^{-3} s^{-1}),

$$\sum_i \left(z_i \frac{\partial J_i}{\partial x} \right) = -r_{\text{ch}}, \tag{3.8}$$

where i runs over all ionic species considered in the model. By using this equation, we do not need to consider the mass balance for the protons and hydroxyl ions, which simplifies the numerical method as the involvement of the protons in all acid-base reactions does not have to be included. However, the production of protons or hydroxyl ions is still calculated correctly.

Next to each master species per group, there is one more unknown in the system; the (dimensionless) electric potential in solution ϕ. Therefore, we need one more equation to fully describe the system. In principle, this could be the Poisson equation, but here we start off with the simpler case of local electroneutrality; at any position in the biofilm, we have zero charge,

$$\sum_i z_i c_i = 0, \tag{3.9}$$

where i runs over all ionic species. This assumption would not hold on a smaller length-scale (on the order of nm) near the electrode, since a charged electrode would result in charge buildup near the electrode. This so called electric double layer would result in a screening of the electric potential at the electrode. However, in this model a larger length-scale (on the order of microns) is considered where local electroneutrality is assumed to hold.

We now have a system of six equations (four mass balance equations (equations 3.7), charge balance (equation 3.8), and local electroneutrality (equation 3.9)) for a total of six unknowns (five master species for each ionic group and the electric potential). Assuming the reaction rates are known (which will be described in section 3.1.2), we would only need appropriate boundary conditions to fully describe the ionic species in the biofilm. Firstly, at the bulk interface ($x = 0$), we take all concentrations to be given by the bulk value,

$$c_i(x = 0) = c_{B,i}, \tag{3.10}$$

with $c_{B,i}$ (mol m^{-3}) the bulk concentration value of species i. With this boundary condition, we assume that no (charged) membrane is present at the biofilm-bulk interface. We also gauge the potential to be zero at the bulk boundary,

$$\phi(x = 0) = 0, \tag{3.11}$$

which can be done once in the system.

Secondly, within each group, there can be no net flux at the electrode boundary. A single species might be involved in a surface reaction, but this flux must always be accompanied by an opposite flux of a species within the same group, resulting in a zero net flux;

$$\sum_j J_j(x = L) = 0, \tag{3.12}$$

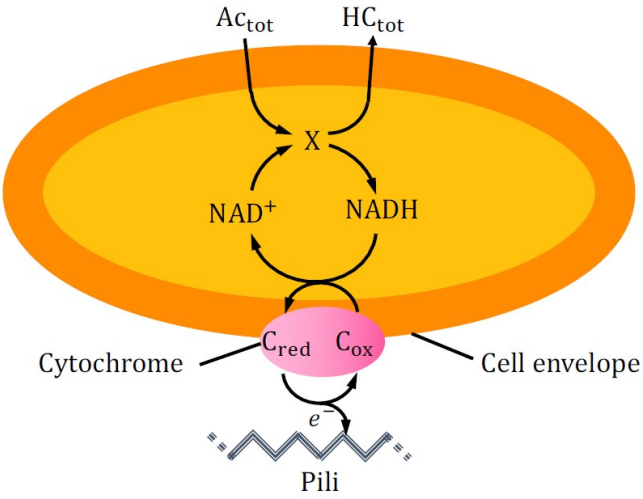

FIGURE 3.2: Overview of the chain of reactions in which acetate species (Ac_{tot}) form an enzymatic complex (X) with NAD^+ (a species found in all living cells capable of accepting electrons) after which NADH can be formed together with bicarbonate species (HC_{tot}). NADH can reduce a cytochrome, after which the reduced cytochrome can transfer an electron to the network of pili. [9]

where j runs over all species within a group. Note that this boundary condition for the group of protons and hydroxyl ions does not need to be included. Instead, we also include that the total ionic current at the electrode boundary must be zero; no ionic current can leave the system through the electrode,

$$\sum_i z_i J_i(x = L) = 0, \tag{3.13}$$

where i runs over all ionic species. This boundary condition implies that only electrons can be transported through the anode; ionic species cannot go through the external circuit.

With these equations and boundary conditions, the system of ionic species is fully determined, once the production rates are all known.

3.1.2 Biochemical reactions

Next to the ionic species present in the aqueous phase, there are bacterial species present within the bacterial cell. The bacterial species present in this model represent a simplified chain of reactions, which results in the creation of excess electrons. This chain can be seen in figure 3.2 and its four reactions will be discussed separately below.

The first biochemical reaction that occurs is the formation of an enzymatic complex, X, consisting of NAD^+ and an acetate species (Ac^- or HAc, grouped as Ac_{tot}). NAD^+ is a common biological molecule, present in all cells [29]. In its reduced form, NADH, it acts as an electron carrier in all kinds of biological processes. The reaction through which this process is modelled is given by

$$Ac_{tot} + 4NAD^+ \overset{r_a}{\rightleftharpoons} 4X, \tag{3.14}$$

with r_a (mol m^{-3} s^{-1}) the rate at which association of X takes place. Note that this reaction does not show exactly which constituent is used. It is only important to

know that for each acetate species that is involved in the reaction, four enzymatic complexes X are formed. By grouping together acetate and acetic acid, we do not need to make assumptions about which molecule is used and since they are linked through an acid-base reaction, the two species are always in equilibrium.

The rate of association is given by a combination of both the forward and backward reaction. Using first-order kinetics, we find

$$r_{\mathrm{a}} = k_{\mathrm{a}}[\mathrm{Ac}]_{\mathrm{tot}} \left[\mathrm{NAD}^{+}\right] - k_{\mathrm{d}}[\mathrm{X}], \tag{3.15}$$

with k_a ($\mathrm{m}^3\ \mathrm{mol}^{-1}\ \mathrm{s}^{-1}$) the rate constant for the association reaction (forward) and k_d (s^{-1}) the rate constant for the dissociation reaction (backward).

The second reaction in the reaction chain is the dissociation of X into $\mathrm{HC}_{\mathrm{tot}}$ and NADH. This reaction is given by

$$4\mathrm{X} \xrightarrow{r_X} 2\mathrm{HC}_{\mathrm{tot}} + 4\mathrm{NADH}, \tag{3.16}$$

with r_X the rate at which X is dissociated. Note that in this model, it is assumed that the backward reaction rate is small compared to the forward reaction and thus can be ignored, rendering the reaction irreversible. This assumption holds if only small concentrations of either $\mathrm{HC}_{\mathrm{tot}}$ or NADH are present. Using first-order kinetics, r_X is given by

$$r_X = k_{\mathrm{X}}[X], \tag{3.17}$$

with k_X (s^{-1}) the rate constant for the dissociation of X.

Reactions 3.14 and 3.16 together form a system in which an enzyme binds to a substrate, after which it is released together with a product. This system has been described in section 2.2.3 and we can define the Michaelis-Menten constant K_M (mol m^{-3}) for the current model, which is given by

$$K_M = \frac{k_{\mathrm{d}} + k_{\mathrm{X}}}{k_{\mathrm{a}}}. \tag{3.18}$$

The two reactions described above provide the connection to the ionic species and give the input for equations 3.7. Therefore, we can now set

$$\begin{aligned} r_{\mathrm{Ac}_{\mathrm{tot}}} &= -r_a \\ r_{\mathrm{HC}_{\mathrm{tot}}} &= r_X \\ r_{\mathrm{H_2P}_{\mathrm{tot}}} &= 0. \end{aligned} \tag{3.19}$$

The next step in the reaction chain is the conversion of transfer of electrons to the cytochromes, which have to go from the oxidized to the reduced form. The actual mechanism by which this happens consists of a number of complex steps involving various proteins, but since we are interested in the physical implications of this reaction, all we need to take into account is that as NADH carries two electrons, two cytochromes can be reduced with one NADH molecule. Therefore, we obtain the following reaction

$$\mathrm{NADH} + 2\mathrm{C}_{\mathrm{ox}} + \mathrm{H}^{+} \overset{r_{\mathrm{cyt}}}{\rightleftharpoons} \mathrm{NAD}^{+} + 2\mathrm{C}_{\mathrm{red}}, \tag{3.20}$$

with r_{cyt} (mol $\mathrm{m}^{-3}\ \mathrm{s}^{-1}$) the reaction rate. Note that the proton within this reaction is present within the bacterial cell and is therefore different from the ionic species discussed before. Since living organisms keep a constant internal environment, we assume the internal proton concentration $[\mathrm{H}_i^{+}]$ (mol m^{-3}) to be at a constant value

of 10^{-4} mol m^{-3} (pH 7). Within the De Lichtervelde model, it is hypothesized that this reaction occurs at a much faster rate than reaction 3.16, which produces NADH and we can therefore assume equilibrium, given by

$$K_{\mathrm{NAD}} = \frac{\left[\mathrm{NAD^+}\right]\left[\mathrm{C_{red}}\right]^2}{\left[\mathrm{NADH}\right]\left[\mathrm{C_{ox}}\right]^2\left[\mathrm{H_i^+}\right]}, \tag{3.21}$$

with K_{NAD} (m^3 mol^{-1}) the equilibrium constant.

In the last reaction, charge accumulated within the cytochromes must be transferred to the network of conductive pili. This is described by the Faradaic equation

$$\mathrm{C_{ox}} + \mathrm{e^-} + \mathrm{H^+} \overset{r_{\mathrm{ch}}}{\rightleftharpoons} \mathrm{C_{red}}, \tag{3.22}$$

with r_{ch} (mol m^{-3} s^{-1}) the reaction rate. The rate at which electrons move from the bacteria to the pili is given by -r_{ch}. In this reaction an electron is present, so we cannot use first-order reaction kinetics to describe the reaction rate, but must instead use a Butler-Volmer equation to take into account the potential in both the pili and the solution. Therefore, the charge transfer rate r_{ch} is given by

$$r_{\mathrm{ch}} = k_{\mathrm{red}}[\mathrm{C}]_{\mathrm{ox}}\left[\mathrm{H^+}\right] e^{-\alpha\Delta\phi} - k_{\mathrm{ox}}[\mathrm{C}]_{\mathrm{red}} e^{(1-\alpha)\Delta\phi}, \tag{3.23}$$

with k_{red} (m^3 mol^{-1} s^{-1}) the rate constant of the reduction, k_{ox} (s^{-1}) the rate constant of the oxidation, α (dimensionless) the transfer coefficient, and $\Delta\phi = \phi_{\mathrm{pili}}(x) - \phi(x)$, with ϕ_{pili} the dimensionless electric potential in the network of pili.

Having described four reactions (reactions 3.14, 3.16, 3.20, and 3.22), we can now set up the dynamics of the five bacterial species. First of all, we note that the total concentration of the NAD-complex, $[NAD]_{tot}$ (consisting of NAD^+, X, and NADH), and the total concentration of the cytochromes, $[C]_{tot}$ (consisting of C_{ox} and C_{red}), are constant and given by

$$\begin{aligned} [\mathrm{NAD}]_{\mathrm{tot}} &= \left[\mathrm{NAD^+}\right] + [\mathrm{NADH}] + [\mathrm{X}] \\ [\mathrm{C}]_{\mathrm{tot}} &= [\mathrm{C}]_{\mathrm{red}} + [\mathrm{C}]_{\mathrm{ox}}. \end{aligned} \tag{3.24}$$

Therefore, we need only three equations to describe the dynamics of the bacterial species. Looking at all four reactions, we find

$$\begin{aligned} \frac{\partial[\mathrm{X}]}{\partial t} &= 4r_{\mathrm{a}} - 4r_{\mathrm{X}} \\ \frac{\partial\left[\mathrm{NAD^+}\right]}{\partial t} &= -4r_{\mathrm{a}} + r_{\mathrm{cyt}} \\ \frac{\partial[\mathrm{C}]_{\mathrm{ox}}}{\partial t} &= -2r_{\mathrm{cyt}} - r_{\mathrm{ch}}. \end{aligned} \tag{3.25}$$

Since we take reaction 3.20 to be in equilibrium, we do not know the expression for r_{cyt}. However, when we look at steady state, where all time derivatives are set to zero, we find that r_{cyt} is actually a dummy variable, which can be removed by a linear combination of the last two equations. Therefore, in steady state, we have a system of five equations (two equations describing the total concentration of the bacterial groups (equations 3.24), two equations from the dynamics of the system (equations 3.25, with a linear combination of the last two), and the equilibrium equation 3.21) and five unknowns, the bacterial species, providing us with a system that can be solved numerically.

3.1.3 Charge transport to the electrode

The final part of the model consists of charge transport through the conductive pili towards the electrode. To describe the current density J_{ch} (A m^{-2}) within the pili, we use Ohm's law, which states that the current density is proportional to the biofilm's electronic conductivity σ_{bf} (S m^{-1}) and the gradient of the electric potential within the pili ϕ_{pili} (dimensionless);

$$J_{\text{ch}} = -\sigma_{\text{bf}} V_T \frac{\partial \phi_{\text{pili}}}{\partial x}. \tag{3.26}$$

Assuming no charge buildup inside the pili, we know that the charge transfer rate must be equal to the divergence of the current density,

$$\frac{\partial J_{\text{ch}}}{\partial x} = r_{\text{ch}} F, \tag{3.27}$$

with F (C mol^{-1}) Faraday's constant, which is needed to obtain the correct dimensions. Combining these two equations we find

$$\sigma_{\text{bf}} V_T \frac{\partial^2 \phi_{\text{pili}}}{\partial x^2} = -r_{\text{ch}} F, \tag{3.28}$$

which describes the pili-potential throughout the biofilm. Since this is a second order differential equation, we must also have two boundary conditions. The first boundary condition is that the potential at the electrode (x = L) is given by the anode overpotential η (V),

$$\phi_{\text{pili}}(x = L) = \frac{\eta}{V_T}. \tag{3.29}$$

The second boundary condition is given by

$$\frac{\partial \phi_{\text{pili}}}{\partial x}(x = 0) = 0, \tag{3.30}$$

which states that no current can go into the bulk ($J_{\text{ch}} = 0$).

Even though the system is fully described by the above model, one more interesting quantity can be obtained, which is the current density at the anode I (A m^{-2}). Since each electron that is transferred to the pili goes to the anode, we can obtain the current density by integrating the charge transfer rate r_{ch} over the biofilm,

$$I = -F \int_0^L r_{\text{ch}}(x) dx. \tag{3.31}$$

This concludes the set-up of the model. In the next section, the numerical methods involved in solving this model are discussed.

3.2 Numerical Methods

In this section, we will discuss how the model can be solved using numerical methods. Within this thesis, MATLAB was used, but the methods can be applied to other types of programming languages as well. The set-up of the program can be roughly divided in four parts, of which three are conducted in an iterative manner. Note that we are interested in steady-state solutions and therefore all time derivatives are set to zero. The dynamics of the system are not described by the current set-up.

The first part of the program contains the initialization. All constant and variables must be defined, a grid must be created, and initial conditions must be implemented. For the current set-up, an equidistant grid suffices, since the scale of interest is the same throughout the biofilm. For the initial conditions, we take constant fields throughout the biofilm. For the ionic species, the boundary conditions can be used, while for the bacterial species, a guess must be made.

After the initialization is complete, an iterative process is created, in which all concentrations and potentials are updated based on the values of the previous iteration. This consists of three main parts; the ionic species and potential, the bacterial species, and the pili potential. For the ionic species and the potential, all biochemical reaction rates (r_{ch}, r_{a}, and r_{X}) are determined using the previous iteration. Next, we can use equations 3.7 together with boundary conditions 3.12, to determine the profile of the total flux of each group ($J_{\text{Ac}_{\text{tot}}} = J_{\text{Ac}^-} + J_{\text{HAc}}$, $J_{\text{HC}_{\text{tot}}} = J_{\text{HCO}_3^-} + J_{\text{H}_2\text{CO}_3}$, and $J_{\text{H}_2\text{P}_{\text{tot}}} = J_{\text{H}_3\text{PO}_4} + J_{\text{H}_2\text{PO}_4^-} + J_{\text{HPO}_4^{2-}}$), since this is given by a first order ordinary differential equation with one boundary conditions (note that the time derivative is set to zero). This can also be done for the ionic current profile $I_{\text{ion}} = \sum_i z_i J_i$, where i runs over all ionic species (equation 3.8 together with B.C. 3.13).

Once the total flux profiles and ionic current profile are known throughout the biofilm, we can determine the concentration of all ionic species. Firstly note that the Na^+ profile can be solved analytically, since we know that for steady state we have $J_{Na^+} = 0$. Using the Nernst-Planck equation (equation 3.1), we then find

$$[\text{Na}](x) = [\text{Na}](0)e^{-\phi(x)}, \tag{3.32}$$

showing that the Na^+ profile is known once the potential throughout the biofilm is known.

To solve for the other ionic species, we substitute the Nernst-Planck equation (equation 3.1) in the total flux and ionic current equations. These equations can be discritized using a central-difference scheme, after which the acid-base equilibria (equations 3.4) can be substituted. Through this substitution, it might appear that we have five unknowns (Ac^-, HCO_3^-, HPO_4^{2-}, H^+, and ϕ), but since we had to discritize first order derivatives, we need to know the concentration at two separate grid points, giving us a total of ten unknowns. Note that for simplicity it is important to first discritize the equations before substituting the acid-base equilibria. These four equations in addition to the local electroneutrality condition (equation 3.9) form one system.

The system of equations can be solved by realizing that for the first grid point, all values are already known due to the boundary conditions (equations 3.10 and 3.11). Therefore, at the second grid point, we only have five unknowns, since we can use the values on the first grid point in our system of equations, resulting in a system of five equations with five unknowns. Therefore, the system can be solved grid point by grid point by using a numerical solver. Once all concentration profiles and the potential are known, we can use the acid-base equilibria and equation 3.32 to determine the concentration profile of all remaining ionic species.

The second main part of the iteration loop focuses on the profiles of the five bacterial species; [NAD^+], [NADH], [X], [C_{ox}], and [C_{red}]. These are also linked together in one system. Firstly, we have two equations describing the total concentration within each group (equations 3.24). Secondly, we have the equilibrium condition given by equation 3.21. Thirdly, equations 3.25 with time derivatives set to zero provide two independent equations (the last two equations can be combined to remove

the dummy variable r_{cyt}). In these last two equations, the expressions for r_a, r_X, and r_{ch} can be substituted. We obtain the following system of equations

$$\begin{aligned}
[\text{NAD}]_{\text{tot}} &= \left[\text{NAD}^+\right] + [\text{NADH}] + [\text{X}] \\
[\text{C}]_{\text{tot}} &= [\text{C}]_{\text{red}} + [\text{C}]_{\text{ox}} \\
K_{\text{NAD}} &= \frac{\left[\text{NAD}^+\right][\text{C}_{\text{red}}]^2}{[\text{NADH}][\text{C}_{\text{ox}}]^2\left[\text{H}_{\text{i}}^+\right]} \\
k_a[\text{Ac}_{\text{tot}}][\text{NAD}] - k_d[\text{X}] &= k_X[\text{X}] \\
8k_a[\text{Ac}_{\text{tot}}][\text{NAD}] - 8k_d[\text{X}] &= -k_{\text{red}}[\text{C}_{\text{Ox}}][\text{H}]e^{-\alpha\Delta\phi} + k_{\text{ox}}[\text{C}_{\text{red}}]e^{(1-\alpha)\Delta\phi},
\end{aligned} \tag{3.33}$$

where the values of ionic species of the previous step can be used and the value of the pili potential from the previous iteration. This system of five equations and five unknowns can then be solved for each grid point.

The last step of the iteration loop focuses on the last unknown, the pili potential. Since we are left with one second order ordinary differential equation (equation 3.28) with two boundary conditions (equations 3.29 and 3.30), this system can be solved in a straightforward manner, where the charge transfer rate r_{ch} from the previous iteration can be used.

This process is iterated until the solution is converged. For this, a condition can be created when the solution can be considered converged. In our case, we have looked at the average charge transfer rate r_{ch} over the entire biofilm, since the charge transfer rate is directly related to the current density I, a property we are interested in. Once the iteration process is finished, this property can be calculated using equation 3.31.

3.3 Results and Discussion

In this section, results obtained from the model described above will be presented. Since this model is a replica from De Lichtervelde *et al.* [9], results can be compared. Firstly, we will look at the current density profile as a function of overpotential, the so-called polarization curves. Secondly, we will present the profile of all ionic species, bacterial species, and both the potential and pili potential at certain fixed parameters. The parameters that are used in each figure can be seen in table 3.1.

In figure 3.3, two polarization curves can be seen. The parameters for these curves were chosen to replicate the two polarization curves of De Lichtervelde *et al.* [9] so that a direct comparison can be made. De Lichtervelde *et al.* [9] have chosen these parameters so that a fit was made with a specific dataset. It must be noted that the curves match the results of De Lichtervelde *et al.* [9] only if k_{ox} is changed by a factor of 10^{-1}. We believe that this was a typographic error. Note that the polarization curves do not go towards the origin. This is because we are specifically looking at an anode, due to reaction 3.16 being irreversible. The backward chain of reactions cannot be followed, making the polarization curve asymmetric. If one would impose a negative overpotential, the curve would simply go to zero current density.

The second type of results are the profiles of each variable for a constant overpotential. This gives insight in what the limiting factor for current production can be within the biofilm. For example, if the number of reduced cytochromes is very high, this is a signal that transfer of electrons to the pili is rate limiting, while if the

TABLE 3.1: The values of all parameters used in the figures (adapted from [9]).

	Biofilm parameters		
L	Thickness	$50^{1,2}$ / 100^{3}	μm
ϵ	Mean porosity	0.9	m^3 AP m^{-3} BF
τ	Mean tortuosity	2.3	m AP m^{-1} BF
K_M	Michaelis-Menten constant	2.2	mol m^{-3}
k_d	Rate constant for dissociation	0.1	s^{-1}
k_X	Rate constant for dissociation of X	0.080^{1} / 0.067^{2} / 0.093^{3}	s^{-1}
K_{NAD}	Equilibrium constant for reaction 3.20	$5000^{1,3}$ / 500^{2}	m^3 mol^{-1}
$[\mathrm{NAD}]_{\mathrm{tot}}$	Total concentration of NAD/NADH components	1	mol m^{-3}
$[\mathrm{C}]_{\mathrm{tot}}$	Total concentration of cytochromes	0.8	mol m^{-3}
k_{red}	Electron transfer constant for reduction	$3.1^{1,3}$ / 4.3^{2}	m^3 mol^{-1} s^{-1}
k_{ox}	Electron transfer constant for oxidation	$0.080^{1,3}$ / $0.059^{2,4}$	s^{-1}
α	Transfer coefficient	0.5	-
σ_{bf}	Biofilm conductivity	0.5	S m^{-1}
η	Overpotential	variable^{1,2} / 0.4^{3}	V
	Diffusion coefficients in free solution (10^{-9} m^2 s^{-1})		
$D_{\mathrm{Ac^-}}$	Acetate	1.09	
D_{HAc}	Acetic acid	1.30	
$D_{\mathrm{HCO_3^-}}$	Bicarbonate	1.18	
$D_{\mathrm{H_2CO_3}}$	Carbonic acid	1.30	
$D_{\mathrm{HPO_4^{2-}}}$	Hydrogen phosphate	0.69	
$D_{\mathrm{H_2PO_4^-}}$	Dihydrogen phosphate	0.85	
$D_{\mathrm{H_3PO_4}}$	Phosporic acid	1.10	
$D_{\mathrm{H^+}}$	Protons	9.31	
$D_{\mathrm{OH^-}}$	Hydroxide	5.27	
$D_{\mathrm{Na^+}}$	Sodium	1.33	
	Acid-Base equilibrium constants		
pK_{HAc}	$\mathrm{HAc} \rightleftharpoons \mathrm{Ac^-} + \mathrm{H^+}$	4.75	mol m^{-3}
$pK_{\mathrm{H_2CO_3}}$	$\mathrm{H_2CO_3} \rightleftharpoons \mathrm{HCO_3^-} + \mathrm{H^+}$	6.35	mol m^{-3}
$pK_{\mathrm{H_3PO_4}}$	$\mathrm{H_3PO_4} \rightleftharpoons \mathrm{H_2PO_4^-} + \mathrm{H^+}$	2.15	mol m^{-3}
$pK_{\mathrm{H_2PO_4^-}}$	$\mathrm{H_2PO_4^-} \rightleftharpoons \mathrm{HPO_4^{2-}} + \mathrm{H^+}$	7.2	mol m^{-3}
pK_{W}	$\mathrm{H_2O} \rightleftharpoons \mathrm{H^+} + \mathrm{OH^-}$	14	mol^2 m^{-6}
	Bulk concentrations (mol m^{-3})		
$[\mathrm{Ac}]_{\mathrm{tot}}$	Total acetate	$20^{1,2}$ / 5^{3}	
$[\mathrm{HC}]_{\mathrm{tot}}$	Total carbonate	$5^{1,2}$ / 2^{3}	
$[\mathrm{H_2P}]_{\mathrm{tot}}$	Total phosphate	$20^{1,2}$ / 5^{3}	
pH		7	

[1] Used in figure 3.3.A.

[2] Used in figure 3.3.B.

[3] Used in figures 3.4, 3.5, 3.6, and 3.7

[4] In [9] a value of 0.59 s^{-1} was given. However, results could only be reproduced for a value of 0.059 s^{-1}. We believe this was a typographic error.

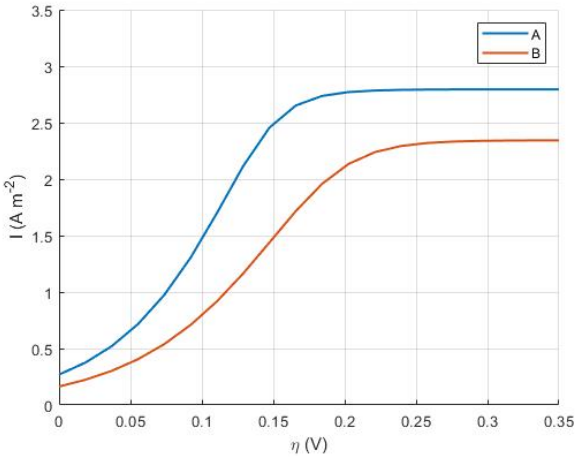

FIGURE 3.3: The current density profile I as a function of overpotential η for two sets of input parameters as given in table 3.1.

pH drops significantly, this is a signal that an accumulation of protons is the limiting factor in the current density that can be extracted from the system. The parameters were chosen such that the bulk solution represents domestic wastewater. In figure 3.4, the steady-state concentration profiles of sodium and the total concentration profile of the acetate, bicarbonate, and phosphate species can be seen. Note that sodium actually represents a group of unreactive ions.

A few observations can be made. Firstly, note that these are steady-state concentration profiles, but not necessarily zero flux profiles. For example, acetate species are continuously used in the chain of reactions, so a constant transport of acetate species is needed to obtain a steady state. However, for sodium, there is no transport since sodium ions are not involved in any reaction. Secondly, observe that even though acetate species are used in the reaction chain, a build-up of acetate is observed at the electrode. Migrational forces thus play an important role within the biofilm. As was concluded by De Lichtervelde *et al.* [9], this shows that mass transfer does not limit the availability of acetate species throughout the biofilm, thus not limiting the current production.

In figure 3.5, the concentration profile of the separate ionic species can be seen. The effect of the acid-base reactions can clearly be seen in these figures, as concentrations start changing rapidly when the pH is at the order of the pK_i value of the acid-base reaction involving species i. For example, we know $pK_{H_2CO_3}$ = 6.35 mol m^{-3} and when the pH is around that value (x $\approx$ 20 μm), the concentrations of HCO_3^- and H_2CO_3 change most rapidly. Also note that the concentration of H_3PO_4 remains close to zero, which can be explained because $pK_{H_3PO_4}$ is equal to 2.15 mol m^{-3} and the pH does not reach that value.

As can be seen in figure 3.5, the pH drops significantly throughout the biofilm. Within this model, it was assumed that the biological chain of reactions was not affected by the pH. However, in literature it has been shown that current production by a certain type of Geobacter bacteria drops significantly at pH 6 and can completely stop at pH 5 [9]. Therefore, De Lichtervelde *et al.* [9] concluded that proton accumulation can inhibit the current production in thick biofilms.

Based on figures 3.3, 3.4, and 3.5, we can conclude that our results are in line with the results from De Lichtervelde *et al.* [9]. Only a small numerical discrepancy can be observed, which could be the result of slightly different numerical methods. To

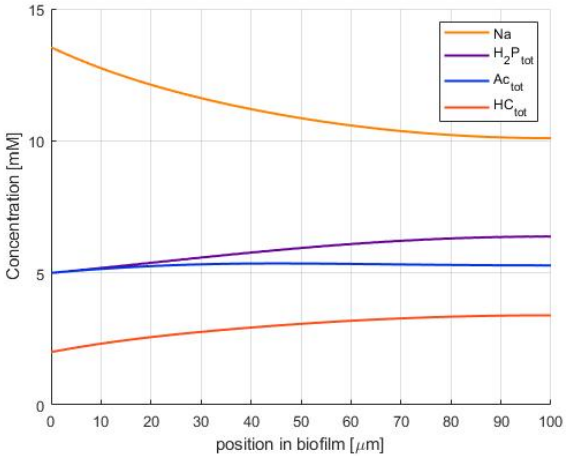

FIGURE 3.4: The steady-state concentration profiles of the acetate (Ac_{tot}), bicarbonate (HC_{tot}), and phosphate (H_2P_{tot}) groups together with the sodium (Na^+) profile throughout the biofilm.

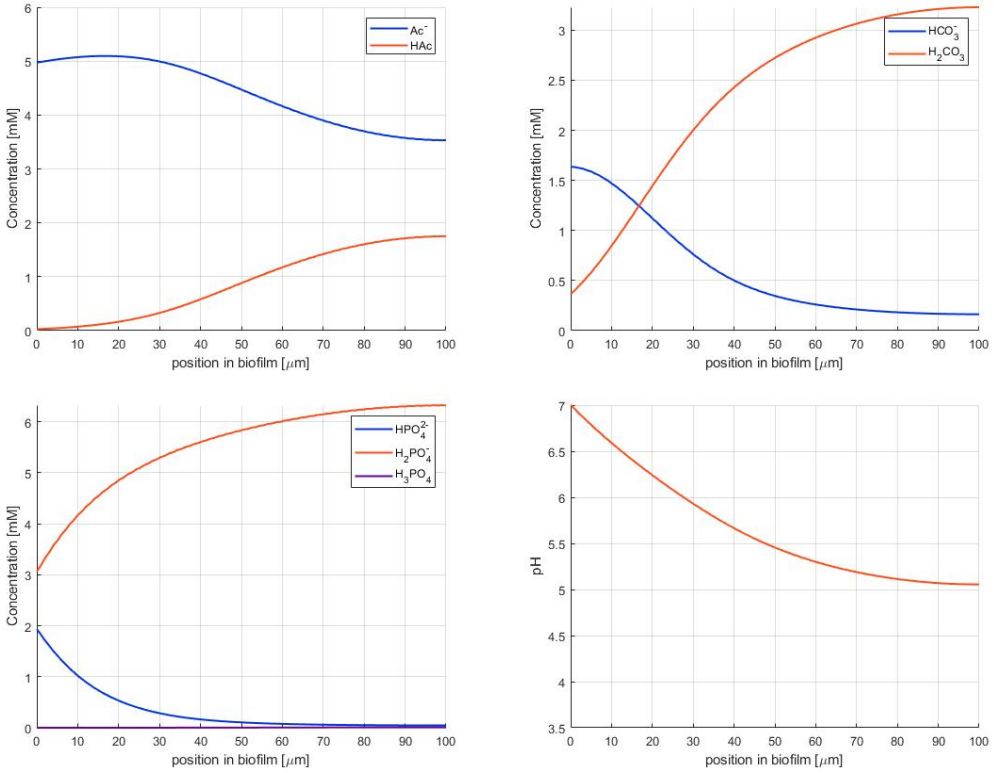

FIGURE 3.5: The steady-state concentration profiles of acetate, bicarbonate, and phosphate species together with the pH profile throughout the biofilm.

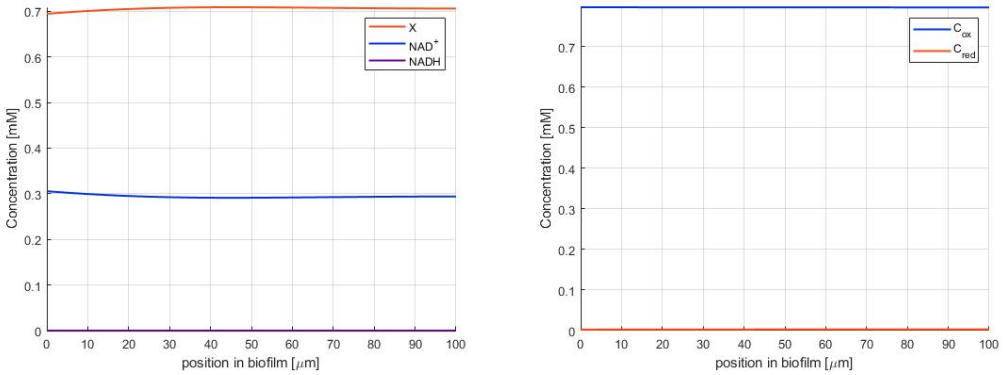

FIGURE 3.6: The steady-state concentration profiles of the NAD-species and cytochromes throughout the biofilm.

get a more thorough overview, we have also included two additional type of figures; the concentration profiles of the bacterial species and the profiles of the potentials.

The concentration profiles of the bacterial species can be seen in figure 3.6. We can see that the concentration of NADH is close to zero, rendering the assumption of irreversibility of reaction 3.16 valid. The low concentration of NADH can be explained from equation 3.21, with K_{NAD} being 5000 m^3 mol^{-1}. Since the internal concentration of protons is fixed at 10^{-4} mol m^{-3}, we can immediately see that the equilibrium position of reaction 3.20 is to the far right. In other words, any NADH molecule that is created is almost immediately converted into NAD^+.

When looking at the concentration profile of the cytochromes, it can clearly be seen that almost all cytochromes are in the oxidized state. From equation 3.23 it can be seen that if the potential difference between the pili and the solution is large, the charge transfer rate r_{ch} becomes negative and reaction 3.22 will go in the backward direction, thus producing an excess of electrons and cytochromes in the oxidized state. Therefore, the large concentration of oxidized cytochromes can be explained by a large potential difference between the pili and the solution. For this we can look at figure 3.7. Note that due to the difference in scale, the two potentials are plotted separately. From this, it is clear that this large potential difference drives reaction 3.22 to the left.

From figure 3.7 a few questions arise that are not immediately clear. Firstly, the curvature of the potential would suggest charge is present within the system. This can be seen from Poisson's equation, which was discussed in section 2.2.2. For a charge neutral system, the Poisson equation has a straight line as solution. One of the conditions that was imposed in the system is that of local electroneutrality, which would imply a straight line in the potential. This discrepancy between local electroneutrality and the Poisson equation cannot be explained straightforwardly. Secondly, at the electrode, the potential in solution is still very small, while the electrode potential was set at 0.4V (roughly 15.8 in units of the thermal voltage). Lastly, since the potential in bulk was set to zero, there is a non-zero slope of the potential at the bulk interface; $\frac{d\phi}{dx}(0) \neq 0$. This would mean charge is present somewhere on the boundary.

The open questions that arise from the potential can only be answered if the local electroneutrality condition is removed and by adding the Poisson equation. By doing so, it can be investigated if an electric double layer has the effect on the potential as is observed in figure 3.7. If there is not a quick drop at the electrode interface, the local electroneutrality condition might not be a valid assumption to

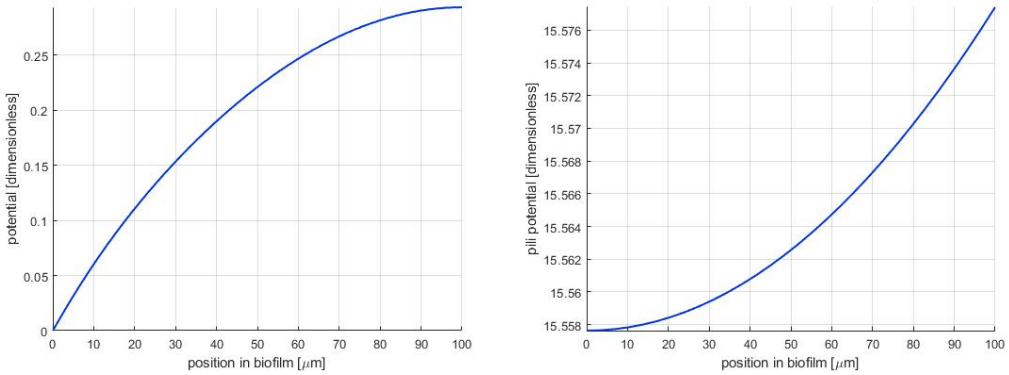

FIGURE 3.7: The steady-state potential and pili potential profiles throughout the biofilm.

work with in systems like the one used here. Therefore, we will make an adaptation to the current model by removing the local electroneutrality condition. This will be discussed in detail in section 4.

4. Releasing the Local Electroneutrality Condition

In this section, we will remove the local electroneutrality condition by instead imposing the one-dimensional Poisson equation, given by

$$\frac{d^2\phi}{dx^2} = -\frac{\rho}{\epsilon V_T}, \tag{4.1}$$

with ρ (C m^{-3}) the local charge density, ϵ the permittivity (F m^{-1}), given by $\epsilon = \epsilon_r \epsilon_0$, with ϵ_r (-) the material dependent relative permittivity and ϵ_0 (F m^{-1}) the vacuum permittivity, and the thermal voltage V_T (V). The Poisson equation is accompanied by two Dirichlet boundary conditions;

$$\begin{aligned} \phi(0) &= 0 \\ \phi(L) &= \frac{\eta}{V_T}, \end{aligned} \tag{4.2}$$

with η (V) the overpotential imposed at the electrode. This equation appears to be quite straightforward, but complicates the overall model significantly. Therefore, an additional assumption can be made. Based on figure 3.7, we assume that a constant pili potential accurately describes the system; the network of pili can be seen as a perfect conductor. This has two advantages. Firstly, it simplifies the model, as equation 3.28 does not have to be included. Secondly, we know that no charge accumulates in a perfect conductor, so the only charge that needs to be included in the charge density of equation 4.1 is the ionic charge. Any electron is assumed to leave the system immediately.

In practice, an electric double layer will form on both the electrode and the network of pili. However, since the model considered here is one-dimensional, creating an electric double layer on the network of pili is not possible. Therefore, we only model the electric double layer at the electrode and make the assumption that the potential drop at the pili due to the electric double layer is of the same order of magnitude as at the electrode. Therefore, we do not need to consider the electric double layer at the pili, ensuring that we can still work in a one-dimensional system.

By adding the Poisson equation, multiple length and time scales must be incorporated. These issues will be discussed in section 4.1. In the next section, section 4.2, the numerical methods needed to solve the system will be discussed. Lastly, some preliminary results will be discussed in section 4.3.

4.1 Length and time scale considerations

By adding the Poisson equation to the system, we expect an electric double layer to appear at the electrode boundary. Since we do not consider a (charged) membrane at the bulk interface, we do not expect an electric double layer at this boundary. The length scale of an electric double layer is a few orders of magnitude smaller than the dominant length scale of the rest of the system, which is on the order of microns.

We can estimate the length scale of the electric double layer by looking at the Debye length λ_D (m), which was obtained from Poisson-Boltzmann theory as discussed in section 2.2.2. For a general electrolyte, the Debye length is given by

$$\lambda_D = \left(\frac{\epsilon k_B T}{e^2 N_A \sum_i c_{b,i} z_i^2} \right)^{1/2}, \tag{4.3}$$

with $c_{b,i}$ (mol m^{-3}) the bulk concentration of species i and where i runs over all ionic species [30]. Note that Avogadro's constant N_A was added to convert molar density into particle density. If we take the bulk concentrations as given in table 3.1, assume each group has a valency of -1, and take the permittivity of water at room temperature ($\epsilon_{r,\text{water}} = 80$), we obtain a Debye length of approximately 3 nm. Note that this is an approximation, since we have taken a valency of -1 within each group, while also charge neutral ions are present.

The Debye length is the length scale on which concentrations will decay to their bulk concentrations. Therefore, a nanometer length scale is important within the electric double layer. Within our system, we need a grid that is on the micron scale throughout the biofilm, while it is on the nanometer scale in the electric double layer (roughly the last tens of nanometers). This will pose challenges in solving the Poisson equation, which will be discussed in section 4.2.

In order to find relevant time scales in the system, we need to find a length squared divided by the diffusion coefficient. The first time scale we consider is the time it takes for an ion to diffuse through the system T_D (s), given by

$$T_D = \frac{L^2}{D_e}, \tag{4.4}$$

with D_e the effective diffusion coefficient, for which we take a value of roughly $5 \cdot 10^{-10}$ m^2 s^{-1}. We then find this diffusion time scale to be in the order of 20 s.

The second time scale we consider is the time it takes for an ion to move through the electric double layer T_{EDL} (s), given by

$$T_{EDL} = \frac{\lambda_D^2}{D_e}, \tag{4.5}$$

which is in the order of 10^{-9} s. The difference in these two time scales has implications for the kind of numerical methods that can be used. This will be discussed in detail in section 4.2.

4.2 Numerical Methods

In this section, the numerical methods needed to solve the system including the Poisson equation will be discussed. The advantages and disadvantages of various approaches will be explained and a recommendation will be made for which method to use.

4.2.1 Solving the one-dimensional Poisson equation

Let us first consider how to solve the one-dimensional Poisson equation. One method is by using matrix inversion [31]. Firstly, the Poisson equation is discretized on an equidistant grid with step size h and N grid points;

$$\phi_{i-1} - 2\phi_i + \phi_{i+1} = h^2 f_i, \quad i = 1, 2, \cdots, N, \tag{4.6}$$

with $f_i = f(x_i) \equiv -\frac{\rho(x_i)}{\epsilon V_T}$, and Dirichlet boundary conditions given at $\phi_0 = \phi(x = 0)$ and $\phi_{N+1} = \phi(x = L)$. Each grid point contributes one equation, giving a system of N equations, which can be written in matrix form;

$$\underbrace{\begin{pmatrix} -2 & 1 & 0 & 0 & 0 & \cdots & \cdots & 0 \\ 1 & -2 & 1 & 0 & 0 & \cdots & \cdots & 0 \\ 0 & 1 & -2 & 1 & 0 & \cdots & \cdots & 0 \\ 0 & 0 & 1 & -2 & 1 & \ddots & \cdots & 0 \\ 0 & 0 & 0 & 1 & -2 & \ddots & \ddots & \vdots \\ \vdots & \vdots & \vdots & \ddots & \ddots & \ddots & \ddots & 0 \\ 0 & 0 & 0 & 0 & \ddots & \ddots & \ddots & 1 \\ 0 & 0 & 0 & 0 & 0 & 0 & 1 & -2 \end{pmatrix}}_{\equiv A} \times \underbrace{\begin{pmatrix} \phi_1 \\ \phi_2 \\ \phi_3 \\ \phi_4 \\ \phi_5 \\ \vdots \\ \phi_{N-1} \\ \phi_N \end{pmatrix}}_{\equiv \Phi} = \underbrace{\begin{pmatrix} h^2 f_1 - \phi_0 \\ h^2 f_2 \\ h^2 f_3 \\ h^2 f_4 \\ h^2 f_5 \\ \vdots \\ h^2 f_{N-1} \\ h^2 f_N - \phi_{N+1} \end{pmatrix}}_{\equiv F}, \tag{4.7}$$

where we haved defined the matrix A and the vectors Φ and F. Note that the boundary conditions appear within vector F. If matrix A can be inverted, we only need to know F and use simple matrix multiplication to obtain the potential at each grid point, $\Phi = A^{-1}F$. It turns out that matrix A can indeed be inverted and its inverse A^{-1} is given by [31]

$$A^{-1} = \frac{-1}{N+1} \begin{pmatrix} N & (N-1) & (N-2) & \cdots & N-(j-1) & \cdots & 3 & 2 & 1 \\ (N-1) & 2(N-1) & 2(N-2) & \cdots & 2[N-(j-1)] & \cdots & 6 & 4 & 2 \\ (N-2) & 2(N-2) & 3(N-2) & \cdots & 3[N-(j-1)] & \cdots & 9 & 6 & 3 \\ \vdots & \vdots & \vdots & \ddots & \vdots & \vdots & \vdots & \vdots & \vdots \\ [N-(i-1)] & 2[N-(i-1)] & 3[N-(i-1)] & \cdots & i[N-(i-1)] & \cdots & 3i & 2i & i \\ \vdots & \vdots & \vdots & \vdots & \vdots & \ddots & \vdots & \vdots & \vdots \\ 3 & 6 & 9 & \cdots & 3j & \cdots & 3(N-2) & 2(N-2) & (N-2) \\ 2 & 4 & 6 & \cdots & 2j & \cdots & 2(N-2) & 2(N-1) & (N-1) \\ 1 & 2 & 3 & \cdots & j & \cdots & (N-2) & (N-1) & N \end{pmatrix}. \tag{4.8}$$

The elements $(a^{-1})_{ij}$ of matrix A^{-1} are given by

$$(a^{-1})_{ij} = \begin{cases} -j\frac{[N-(i-1)]}{N+1}, & i \geq j \\ -i\frac{[N-(j-1)]}{N+1}, & i < j. \end{cases} \tag{4.9}$$

Now that we know the inverse, we can simply solve for the potential at each grid point, which is given by

$$\begin{aligned} \phi_i = (a^{-1})_{ij} F_j = \frac{-h^2}{N+1} \Bigg[\sum_{j=1}^{i} j(N-(i-1)) f_j - (N-(i-1)) \frac{\phi_0}{h^2} + \\ \sum_{j=i+1}^{N} i(N-(j-1)) f_j - i\frac{\phi_{N+1}}{h^2} \Bigg]. \end{aligned} \tag{4.10}$$

We can use equation 4.10 to determine the potential at each point for a given charge distribution and using an equidistant grid. However, as indicated in section 4.1, in our system, we have two relevant length scales. At the electrode we need a nm

sized grid, while throughout the rest of the biofilm, we need a μm sized grid. A few methods were investigated to solve the Poisson equation on a non-equidistant grid, of which one gives accurate results. The few methods that did not give reliable results are briefly discussed in appendix A. Below, the method that gives accurate results is presented.

Based on the analysis of appendix A, we cannot use two separate grid sizes in our system. Therefore, we must use an equidistant grid on the nm scale throughout the entire biofilm. However, calculating all variables at each grid point takes too long for any practical application. This is the main reason for needing two grids. The solution to obtain a nm sized grid at the edge whereas having a μm sized grid in the biofilm, while still having an equidistant grid to be able to solve the Poisson equation is by defining a nm sized grid throughout the entire system on which the Poisson equation can be solved, but only calculating the ionic species every 1000 grid points. For every grid point in between, one can solve the Poisson equation in which the charge density for each point is determined by taking a linear function connecting the charge densities at the points where the ionic species are calculated. Since the potential can be calculated using simple multiplication, this does not slow down the program significantly, making this both a fast and accurate approach in solving the one-dimensional Poisson equation.

4.2.2 Set-up of the model

Having a method of solving the one-dimensional Poisson equation, we can now change our model set-up. Two main changes must be made. Firstly, the last part of the iterative loop, as described in section 3.2, in which the pili potential is calculated can be removed. As explained before, we assume a perfect conducting network of pili, thus having no pili potential drop over the biofilm. Instead, the pili potential is equal to the anode overpotential throughout the entire biofilm.

Secondly, the potential must be calculated separately from the ionic species. In the original model, we obtained one system of equations containing all ionic species and the potential. However, we must now use the Poisson equation to obtain the potential throughout the biofilm. Therefore, we first determine the concentration profile of all ionic species using the system of equations from the original model without the local electroneutrality condition and using the potential from the previous iteration. From these concentration profiles, the charge density profile is calculated, which can be used to solve for the potential using the Poisson equation. If needed, we can iterate the process of calculating the profiles of the ionic species and the potential until both profiles are converged.

There are still two different methods of solving the model, a stationary-state method, as done with the original model, or a time-dependent method. In the time-dependent set-up, all time-derivatives have to be discritized as well. This makes the iteration process a time evolution of the system. The advantage of using the time-dependent method is that the charge density changes slowly, giving a more stable behaviour of the potential. In order to assess the viability of this method, we can look at the time scales that we identified. The time it takes for an ion to move through the Debye length is roughly 10^{-9} s. This is the step size that must be taken in order to have a stable time-evolution of the system. For larger time steps, the charge density changes too rapidly, resulting in inaccurate potential profiles. However, the diffusion time T_D is approximately 20 s. Therefore, in order to have particles from the bulk move through the system to add to the electric double layer, we need roughly 10^{10} iteration loops. This huge number of iterations results in a program which takes

a very long time to reach a steady-state solution. Therefore, even though this method would give accurate results, the program must run for too long to have any results, rendering this method not useful.

We must use the stationary-state method to obtain any results for this model, as was done with the original model. However, some caution in determining the potential must be taken. Take for example a Poisson-Boltzmann distribution of the ionic species. Ions with valency -1 will then have a concentration near the electrode, where $\phi \approx 15$, that is $e^{15} \approx 10^6$ times larger than their bulk concentration, while sodium will have a concentration that is $e^{-15} \approx 10^{-7}$ times larger than its bulk concentration, giving a difference in concentration of approximately 10^6 mol m^{-3}. This corresponds to a charge density of $\rho = eN_A \cdot 10^6 \approx 10^{11}$ C m^{-3}. Looking at equation 4.10, using a grid size of $h = 1$ nm and $f = -\frac{\rho}{\epsilon V_T} \approx 10^{21}$ m^{-2}, we can say that in one grid point, the potential changes by roughly $h^2 f \approx 10^3$. Within one grid point, the potential drops below zero. This shows that the system is unstable. Initial conditions close to the expected result, an electric double layer of roughly 3 nm, might prevent this from happening. Additionally, a mixing parameter β can be introduced, which indicates how much of the new concentrations must be kept. For example, a mixing parameter of 0.9 means that 90% of the calculated concentrations and 10% of the concentrations from the previous iteration are combined. This results in a more stable system, which needs more iterations to converge, however.

It is important to realize that the large concentrations do not appear in the physical system. The Nernst-Planck equation that is used only holds in the dilute limit, making the results within the electric double layer questionable. However, we are interested in the profile of the potential, which should be represented accurately.

4.3 Results and Discussion

Based on the numerical methods as discussed in the previous section, the created program does not yet produce reliable results. Therefore, we cannot compare this model to the original model. However, we have already learned more about the system by investigating how the Poisson equation would need to be included. Based on length scale considerations, we found that the electric double layer would only be a few nm thick. A drop in the dimensionless potential to 0.3, as observed in figure 3.7, could be achieved within roughly 10 nm. Outside of the electric double layer, negative and positive charges will roughly be in balance, giving (local) charge neutrality. Therefore, the results from the original model are not unreasonable, if one simply assumes that an exponential tail is present at the end of the potential profile.

One must still be cautious with using the curve of the potential, figure 3.7. Even though the sudden drop in potential at the electrode can be explained with the formation of an electric double layer, the curvature of the potential would still indicate charge being present in the system, while the local electroneutrality condition assumes no charge in the system. Therefore, it is advised to not draw conclusions based on the potential profile.

5. Discussion and Conclusion

In this thesis, we have presented a model to describe the processes happening within a biofilm. The main focus was on doing this from a physics perspective; transport equations linked to (bio)chemical reactions were key in modelling the biofilm. In section 3, we were able to recreate the results from De Lichtervelde *et al.* [9], showing that this model can be reproduced. However, the potential profile appeared to be inconsistent with the Poisson equation; no charge was present in the system, but the potential was not a straight line. In addition, the potential did not approach the overpotential near the electrode.

In section 4 we created an approach for adding the Poisson equation to the model. This gave a first indication to the question raised in the introduction; is the local electroneutrality condition consistent with the results that were obtained from the original model? Even though results from the adapted model were not yet reliable, an analysis of the Debye length for the system showed that the results from the original model were not implausible. However, it still remains a question what the potential throughout the biofilm looks like.

In order to learn more about the system, it is recommended that the model using the Poisson equation is stabilized, giving results of the profiles in the electric double layer. In addition, the model can be extended by including laminar flow of the bulk system, thus recreating a more realistic wastewater stream. By making the model two-dimensional, additional challenges arise, such as how the network of pili should be described in a two-dimensional manner. Electric double layers on this network of pili can even be included.

The model that is created here can also benefit from a more extensive biological approach. In section 3, it was shown that the pH throughout the biofilm decreases significantly, which has an impact on the functioning of the bacteria. However, if the bacteria within the biofilm do not produce an excess of electrons, they also do not produce additional protons. Therefore, if the decrease in functioning of the bacteria due to a proton build up is taken into consideration, it might be that the accumulation of protons decreases. It would be interesting to model this interplay.

In conclusion, the technology of bioelectrochemical systems has the potential to be implemented on a large scale, once more improvements are made. Experimental research can build upon the theoretical approach taken here in order to optimize specific systems. In addition, the current work has provided a more fundamental understanding of the physical processes within the biofilm.

6. Acknowledgements

I would like to thank my supervisor Prof. dr. René van Roij for his help and supervision during this research project. His enthusiasm and input has helped me in creating the results as presented here. In addition, I would like to express my gratitude to dr. Dysktra, one of the creators of the original biofilm model. He offered to answer questions and in doing so, helped me move forward with recreating his results. Lastly, I would like to thank the members of the Soft Matter Group for asking critical questions and providing additional ideas.

A. The one-dimensional Poisson equation

In this appendix, various unsuccessful approaches to solving the one-dimensional Poisson equation on two separate grids are presented. On an equidistant grid, the discretized Poisson equation is given by

$$\phi_{i-1} - 2\phi_i + \phi_{i+1} = h^2 f_i, \quad i = 1, 2, \cdots, N, \tag{A.1}$$

with $f_i = f(x_i) \equiv -\frac{\rho(x_i)}{\epsilon V_T}$, and Dirichlet boundary conditions given at $\phi_0 = \phi(x = 0)$ and $\phi_{N+1} = \phi(x = L)$. Next we consider how to extend this to a non-equidistant grid.

Consider two grids with different grid sizes. For grid points 1, ..., N_1 a grid size h_1 is used, whereas for grid points $N_1 + 1$, ..., $N_1 + N_2 = N$ a grid size h_2 is used. We have Dirichlet boundary conditions given at both edges (ϕ_0 and ϕ_N), but not in between the two grids. A first approach to solving the Poisson equation on these grids, is by using grid point $N_1 + 1$ as boundary condition for the first grid, and grid point N_1 as boundary condition for the second grid. The boundary condition for the first grid would be given by

$$\phi_{N_1+1} = \frac{-h_2^2}{N_2 + 1}\left[N_2 f_{N_1+1} - N_2\frac{\phi_{N_1}}{h_2^2} + \sum_{j=2}^{N_1+N_2}(N_2 - (j-1))f_{N_1+j} - \frac{\phi_N}{h_2^2}\right], \tag{A.2}$$

which still depends on ϕ_{N_1}. By substituting this into the expression for ϕ_{N_1}, one can solve for ϕ_{N_1}. This value can then be used in equation A.2 to solve for ϕ_{N_1+1}. We would then have both intermediate boundary conditions and the rest of the system can be solved. However, there is one issue with this approach, rendering results wrong. Looking at equation 4.7, it becomes clear that the boundary conditions need to be at distance h from the first/final grid point. For the second grid, this is the case; intermediate boundary condition ϕ_{N_1} and right boundary condition ϕ_N are both separated from the grid by a distance h_2. However, for the first grid this is not the case. The left boundary condition is at a distance h_1 from grid point 1, whereas the intermediate boundary condition ϕ_{N_1+1} is at a distance h_2 from grid point N_1. This difference makes the use of equation 4.7 invalid, as factors of h_1 and h_2 would need to be included in the last row of matrix A. This would make the inversion impossible. In conclusion, we cannot use this approach.

A second approach would be to adapt the two grids in such a manner that boundary conditions can be chosen which are located at the same distance as the grid size. One method to achieve this is by having the second grid within the final grid point of the first grid. The first grid consists of N_1 grid points with grid size h_1. The second grid consists of N_2 grid points with grid size $h_1/(N_2 + 1)$. The distance between grid point N_1 and boundary condition ϕ_N would be exactly h_1. Therefore, we can still use both boundary conditions (ϕ_0 and ϕ_N) to solve for the Poisson equation on the first grid. We would instead need to adapt the value of f_{N_1} to incorporate the charge density profile on the second grid. Two options are possible; taking the total charge density or the average charge density over grid points N_1

up to and including $N_1 + N_2$. Once the potential is known on the first grid, ϕ_{N_1} can be used as boundary condition for solving the second grid. However, the results on the first grid are unreliable. The multiplication scheme between the matrix elements a_{ij}^{-1} and f_j as can be seen in equation 4.10 is lost by both manners of adapting f_{N_1}. This approach cannot be used.

A third approach is to consider the Poisson equation explicitly at the boundary between the two grids. Using a central difference scheme, the Poisson equation at the boundary is given by

$$\frac{1}{h_1 + h_2}\left[\frac{2\phi_{N_1+1}}{h_2} - 2(\frac{1}{h_1} + \frac{1}{h_2})\phi_{N_1} + \frac{2\phi_{N_1-1}}{h_1}\right] = f_{N_1}. \tag{A.3}$$

We can substitute equation A.2 into equation A.3 to get rid of ϕ_{N_1+1}. However, we cannot get rid of ϕ_{N_1-1} to be able to solve for ϕ_{N_1}, because we run into the same problem; we do not have a well-defined right boundary condition for the first grid. We cannot use this approach as well.

Any set-up with two grids eventually results in the same issue; no accurate intermediate boundary conditions can be created. Therefore, we conclude that we must solve the Poisson equation using an equidistant grid.

Bibliography

[1] United Nations (UN), *Transforming our world: The 2030 agenda for sustainable development*, [Online; accessed 28-September-2020], 2015. [Online]. Available: https://sustainabledevelopment.un.org/content/documents/21252030\%20Agenda\%20for\%20Sustainable\%20Development\%20web.pdf.

[2] R. A. Rozendal, H. V. Hamelers, K. Rabaey, J. Keller, and C. J. Buisman, "Towards practical implementation of bioelectrochemical wastewater treatment," *Trends in biotechnology*, vol. 26, no. 8, pp. 450–459, 2008.

[3] T. H. Sleutels, A. Ter Heijne, C. J. Buisman, and H. V. Hamelers, "Bioelectrochemical systems: An outlook for practical applications," *ChemSusChem*, vol. 5, no. 6, pp. 1012–1019, 2012.

[4] K. Rabaey, L. Angenent, U. Schroder, and J. Keller, *Bioelectrochemical systems*. IWA publishing, 2009.

[5] B. E. Logan, "Scaling up microbial fuel cells and other bioelectrochemical systems," *Applied microbiology and biotechnology*, vol. 85, no. 6, pp. 1665–1671, 2010.

[6] B. E. Logan, R. Rossi, P. E. Saikaly, *et al.*, "Electroactive microorganisms in bioelectrochemical systems," *Nature Reviews Microbiology*, vol. 17, no. 5, pp. 307–319, 2019.

[7] P. Clauwaert, P. Aelterman, L. De Schamphelaire, M. Carballa, K. Rabaey, W. Verstraete, *et al.*, "Minimizing losses in bio-electrochemical systems: The road to applications," *Applied microbiology and biotechnology*, vol. 79, no. 6, pp. 901–913, 2008.

[8] H. V. Hamelers, A. Ter Heijne, T. H. Sleutels, A. W. Jeremiasse, D. P. Strik, and C. J. Buisman, "New applications and performance of bioelectrochemical systems," *Applied microbiology and biotechnology*, vol. 85, no. 6, pp. 1673–1685, 2010.

[9] A. De Lichtervelde, A Ter Heijne, H. Hamelers, P. Biesheuvel, and J. Dykstra, "Theory of ion and electron transport coupled with biochemical conversions in an electroactive biofilm," *Physical Review Applied*, vol. 12, no. 1, p. 014 018, 2019.

[10] V. S. Bagotsky, *Fuel cells: problems and solutions*. John Wiley & Sons, 2012, vol. 56.

[11] Wikimedia Commons, *File:galvanic cell labeled.svg — wikimedia commons, the free media repository*, [Online; accessed 6-October-2020], 2020. [Online]. Available: https://commons.wikimedia.org/w/index.php?title=File:Galvanic_cell_labeled.svg&oldid=473329324.

[12] Wikimedia Commons, *File:solid oxide fuel cell protonic.svg — wikimedia commons, the free media repository*, [Online; accessed 6-October-2020], 2020. [Online]. Available: https://commons.wikimedia.org/w/index.php?title=File:Solid_oxide_fuel_cell_protonic.svg&oldid=458654463.

[13] R. O'hayre, S.-W. Cha, W. Colella, and F. B. Prinz, *Fuel cell fundamentals*. John Wiley & Sons, 2016.

[14] M.-C. Pera, D. Hissel, H. Gualous, and C. Turpin, *Electrochemical components*. John Wiley & Sons, 2013.

[15] N. S. Malvankar, M. Vargas, K. P. Nevin, A. E. Franks, C. Leang, B.-C. Kim, K. Inoue, T. Mester, S. F. Covalla, J. P. Johnson, *et al.*, "Tunable metallic-like conductivity in microbial nanowire networks," *Nature nanotechnology*, vol. 6, no. 9, pp. 573–579, 2011.

[16] G. D. Schrott, P. S. Bonanni, L. Robuschi, A. Esteve-Nuñez, and J. P. Busalmen, "Electrochemical insight into the mechanism of electron transport in biofilms of geobacter sulfurreducens," *Electrochimica acta*, vol. 56, no. 28, pp. 10 791–10 795, 2011.

[17] R. Y. Adhikari, N. S. Malvankar, M. T. Tuominen, and D. R. Lovley, "Conductivity of individual geobacter pili," *RSC advances*, vol. 6, no. 10, pp. 8354–8357, 2016.

[18] A. E. Franks, K. P. Nevin, R. H. Glaven, and D. R. Lovley, "Microtoming coupled to microarray analysis to evaluate the spatial metabolic status of geobacter sulfurreducens biofilms," *The ISME journal*, vol. 4, no. 4, pp. 509–519, 2010.

[19] P. J. Mouser, D. E. Holmes, L. A. Perpetua, R. DiDonato, B. Postier, A. Liu, and D. R. Lovley, "Quantifying expression of geobacter spp. oxidative stress genes in pure culture and during in situ uranium bioremediation," *The ISME Journal*, vol. 3, no. 4, pp. 454–465, 2009.

[20] R. van Roij, *Soft condensed matter theory; lecture notes*. Utrecht University, 2018.

[21] R. Maex, "On the nernst–planck equation," *Journal of Integrative Neuroscience*, vol. 16, no. 1, pp. 73–91, 2017.

[22] J. E. House, *Principles of chemical kinetics*. Academic Press, 2007.

[23] R. Chang, *Physical chemistry for the biosciences*. University Science Books, 2005.

[24] K. Kontturi, L. Murtomäki, and J. A. Manzanares, *Ionic transport processes: in electrochemistry and membrane science*. OUP Oxford, 2008.

[25] M. Z. Bazant, *Reaction kinetics; lecture notes*. MIT, 2011.

[26] A. J. Bard, L. R. Faulkner, *et al.*, "Fundamentals and applications," *Electrochemical Methods*, vol. 2, no. 482, pp. 580–632, 2001.

[27] M. Rini, B.-Z. Magnes, E. Pines, and E. T. Nibbering, "Real-time observation of bimodal proton transfer in acid-base pairs in water," *Science*, vol. 301, no. 5631, pp. 349–352, 2003.

[28] K. J. Powell, P. L. Brown, R. H. Byrne, T. Gajda, G. Hefter, S. Sjöberg, and H. Wanner, "Chemical speciation of environmentally significant heavy metals with inorganic ligands. part 1: The hg2+–cl–, oh–, co32–, so42–, and po43– aqueous systems (iupac technical report)," *Pure and applied chemistry*, vol. 77, no. 4, pp. 739–800, 2005.

[29] N. Pollak, C. Dölle, and M. Ziegler, "The power to reduce: Pyridine nucleotides - small molecules with a multitude of functions," *Biochemical Journal*, vol. 402, no. 2, pp. 205–218, 2007.

[30] R. Tadmor, E. Hernández-Zapata, N. Chen, P. Pincus, and J. N. Israelachvili, "Debye length and double-layer forces in polyelectrolyte solutions," *Macromolecules*, vol. 35, no. 6, pp. 2380–2388, 2002.

[31] S. B. Gueye, "The exact formulation of the inverse of the tridiagonal matrix for solving the 1d poisson equation with the finite difference method," *Journal of Electromagnetic Analysis and Applications*, vol. 6, no. 10, pp. 303–308, 2014.